On the Dynamics and Evolution of Self-Propelled Particle Models



Christian Yates
Somerville College
University of Oxford

A thesis submitted for the degree of
Master of Science in Mathematical Modelling and Scientific Computing
7th of September 2007

Supervisors:
Professor David Sumpter, University of Uppsala
Dr Radek Erban, University of Oxford
Professor Carlos Escudero, University of Oxford

Acknowledgements

There are several individuals and institutions who have assisted me in one way or another in the completion of this project, to whom I would like to express my gratitude.

Firstly I would like to thank my supervisors for helping me discover exciting areas of mathematics which, up until recently, were unknown to me. Their suggestions and guidance throughout the project have been most appreciated. I would specifically like to thank David Sumpter for looking after me on my visit to Sweden. Doing mathematics in a foreign country for the first time can be daunting, so thank you for making me feel at home. On a related note I would like to record my debt to both the Universities of Oxford and Uppsala for generously funding that visit, which contributed hugely to the completion of the project. I must also thank the EPSRC, for funding me through the MSc. I would like thank my family and friends who have supported me over the course of the last year even when I have been little fun to be around. Finally I would like to thank my Dad, to whose generous support and encouragement over the last 22 years I owe a lot.

"Bring forward what is true.
Write it so that it is clear.
Defend it to your last breath!"
Ludwig Eduard Boltzmann (1844-1906)

Contents

1 Introduction **1**
- 1.1 Motivation and Aims . . . 1
- 1.2 Summary of Original Results . . . 5

2 Stochastic Switching **6**
- 2.1 Brownian Motion . . . 6
- 2.2 Stochastic Integration . . . 7
- 2.3 The Euler-Maruyama Method . . . 8
- 2.4 Applying the Numerical Method to an Example . . . 9
- 2.5 The Fokker-Planck Equation . . . 11
- 2.6 Stationary Probability Distribution . . . 14
- 2.7 Moments of the First Passage Time . . . 16
- 2.8 Mean Switching Times . . . 20
- 2.9 Equation-Free Analysis . . . 22

3 Self-Propelled Particle Models **26**
- 3.1 Variation of Alignment with Interaction Radius . . . 26
- 3.2 One-Dimensional Model . . . 28
- 3.3 Application of the Equation-Free Method to the One Dimensional Model . . . 30
- 3.4 Application of the Equation-Free Method to the Full Interaction SPP Model 33
- 3.5 Long-Time Equation-Free Analysis . . . 36

4 Evolutionary Game Theory **41**
- 4.1 Conflicts . . . 41
- 4.2 Other Types of Game . . . 43
- 4.3 Evolutionary Stability . . . 44
- 4.4 Nash Equilibria . . . 45
- 4.5 Evolutionarily Stable Strategies . . . 45
- 4.6 The Replicator Equation . . . 46
- 4.7 Other Types of Game Revisited . . . 47
- 4.8 Optimal Strategy Versus Evolutionarily Stable Strategy . . . 48

5 Two-Dimensional Model **50**
- 5.1 Optimal Radius for Following the Leader . . . 51
- 5.2 Investigation into The Evolutionarily Stable Radius for Following the Leader 54

6 Conclusions **58**
- 6.1 Further Work . . . 60

7 Appendices **A**
7.1 Appendix A-Derivation of the Backwards Kolmogorov Equation . . . . . A
7.2 Appendix B-Further Investigation into the Evolutionarily Stable Radius . . B

References **I**

List of Figures

1.1 *Change in Φ^t over time for three different locust densities. (A) 7 (or 3.47 moving on average), (B) 20 (or 12.05 moving on average), and (C) 60 (or 47.35 moving on average) locusts [4].* 2

2.1 *An example of a simple Brownian path with $dt = 0.002$.* 7
2.2 *The chosen potential for the SDE (2.3.2): $\phi(x) = 10(\frac{x^4}{4} - \frac{x^2}{2})$.* 10
2.3 *Experimental results (A) compared with the numerical solution of the chosen SDE (B). (Note Figure 1.1 (B) has been renamed (A) in this figure.)* 10
2.4 *Two methods of finding the SPD.* 16
2.5 *Equation-free approximations to the drift and diffusion terms of SDE (2.9.1) plotted with the actual drift and diffusion terms. NOTE: Scales on the y-axis are not the same for plots (A), (B), (C) and (D).* 24
2.6 *Equation-free approximation to the potential plotted with the real potential.* 25

3.1 *Variation of the alignment, $\zeta_{overall}$, for a one dimensional SPP model with the IR of the particles.* 28
3.2 *A plot of $G(u)$ versus u for $-3 \leq u \leq 3$ and with $\beta = 1$.* 29
3.3 *A surface plot of alignment varying with IR, r and weighting parameter, α.* 30
3.4 *(A)The position of each particle at each time step. (B) Un-normalised alignment, ζ varies with time.* 31
3.5 *(A) Experimental and (B) modelled results for locust density $\rho = 1$.* 32
3.6 *The diffusion and drift and potential for the Czirók model found using equation-free techniques.* 32
3.7 *(A)The potential for the Czirók model found using the equation-free technique. (B) SPD for the Czirók model found using the equation-free technique compared to the SPD found using the histogram method (originally described for Figure 2.4).* 33
3.8 *The potential and SPD for a special case of the Czirók model (the IR covers the whole domain).* 36
3.9 *The diffusion and drift terms of the SDE supposedly underlying alignment of the particles in the model, calculated using the long-time equation-free technique.* 37
3.10 *The potential and SPD derived using the long-time equation-free technique.* 37
3.11 *A comparison of the diffusion, drift and potential of an assumed underlying SDE for alignment of the particles in the Czirók model derived using the two equation-free methods.* 38
3.12 *Switching behaviour demonstrated in the sand ring experiment by Buhl et al with 25 locusts.* 39
3.13 *(A) The potential for an experiment using the same techniques as in [4] but with 25 locusts. (B) A different scaling and cropping of figure (A).* 39
3.14 *Figure (A) shows two approximations to the SPD for the experiment with 25 locusts. Figure (B) shows three different methods of finding the SPD of the example SDE for a short-time simulation.* 40

4.1 *The four different qualitative behaviours of the cooperate defect game.* 48

5.1 *Varying alignments of the particles in the two dimensional model plotted as a surface for varying r and α with noise parameter $\eta = 2$, population size $N = 80$ and domain size $L = 25$.* 54
5.2 *A surface plot to show pictorially the values of the number of successful invasions when one interaction radius attempts to invade the majority of another.* 56

List of Tables

2.1 *Mean switching time evaluated using four different methods.* 22

3.1 *A comparison of two methods of finding the mean switching time for the Czirók model with noise $\eta = 3$, density $\rho = \frac{1}{3}$ particles per unit length and IR, $r = 4$.* 33

4.1 *Payoff matrix for the 'hawk-dove' game.* 42
4.2 *Payoff matrix for cooperate-defect games.* 43
4.3 *Normalised payoff matrix for cooperate-defect games.* 44
4.4 *Normalised payoff matrix for the general cooperate-defect game.* 47

5.1 *A table to demonstrate strategy invasion over a large range of IR.* 55

7.1 *A table to demonstrate strategy invasion between smaller IR.* . . . . . B

Chapter 1

Introduction

This project is divided in to two different but overlapping segments. The first segment (Chapters 2 and 3) deals with the dynamics of one dimensional self-propelled particle (SPP) models. The second segment (Chapters 4 and 5) deals with the evolution of two dimensional SPP models. In both areas I aim to give a broad introduction to the models and the relevant mathematical techniques that will accompany them. I will then use both the models and the techniques to recreate and create afresh interesting results in the relevant areas.

1.1 Motivation and Aims

During quiet periods (known as recessions) desert locusts are usually restricted to the semi-arid and arid deserts of Africa, the Near East and South-West Asia that receive less than 200 mm of rain annually. This is an area of about 16 million square kilometres, consisting of parts of 30 countries. However, during plagues, desert locusts may spread over an enormous area of some 29 million square kilometres, extending over or into parts of 60 countries. This is more than 20% of the total land surface of the world. During plagues, the desert locust has the potential to damage the livelihood of a tenth of the world's population [12].

In recent models from theoretical physics it has been predicted that mass migrating animal groups may share group level properties irrespective of the type of animals in the group. One of the predictions is that as the density of animals increases a transition occurs from disordered movement of individuals in a group to highly aligned collective motion. Understanding this phenomenon is important in order to be able to control mobile swarming pests, such as desert locusts, which have a devastating socio-economic impact on humans. In their paper [4] Buhl et al confirmed the prediction of a rapid transition from ordered to disordered movement and identified a critical density for the onset of coordinated marching in locust nymphs (wingless juveniles). They also demonstrated a dynamic instability in motion at densities typical of locusts in the field, in which groups can switch direction without external perturbation, potentially facilitating the rapid transfer of directional information [4].

In their experiment different numbers of third-instar[1] locusts ranging from 5 to 120 insects (corresponding to densities of 12.3 to 295 locusts/m^2) were placed in a ring-shaped

[1]Term for a developing locust after the third shedding of the skin.

arena. Their positions were recorded for 8 hours using a digital camera. Movies were processed with tracking software that computed the position and orientation of each locust. The orientation, χ, of a locust is defined as the smallest angle between one line drawn between the locust's two consecutive positions and a second line drawn from the centre of the arena to the locust's first position. Hence χ varies between $-\frac{\pi}{2}$ and $\frac{\pi}{2}$. For each locust i, an orientation χ_i^t was calculated at each camera image or time step t. This was then used to calculate the instantaneous alignment Φ^t as the normalised average of the orientation for all moving locusts:

$$\Phi^t = \frac{2}{m\pi} \sum_{i=1}^{m} \chi_i^t, \tag{1.1.1}$$

where m is the total number of moving locusts. Values of Φ^t close to the extremal values of 1 and -1 indicate the alignment of all the locusts in the same direction, whereas values close to zero indicate an absence of any collective alignment [4]. It was found that the coordinated marching behaviour depended strongly on locust density. At low densities (2 to 7 moving locusts or 5.3 to 17.2 locusts/m^2) there was low incidence of alignment among individuals. Intermediate densities (10 to 25 moving locusts or 24.6 to 61.5 locusts/m^2) were characterised by long periods of collective rotational motion with rapid spontaneous changes in direction. At densities above 73.8 locusts/m^2 (30 or more moving locusts) spontaneous changes in direction did not occur within the timescale of the observations. The locusts quickly adopted a common and persistent rotational direction (see Figure 1.1).

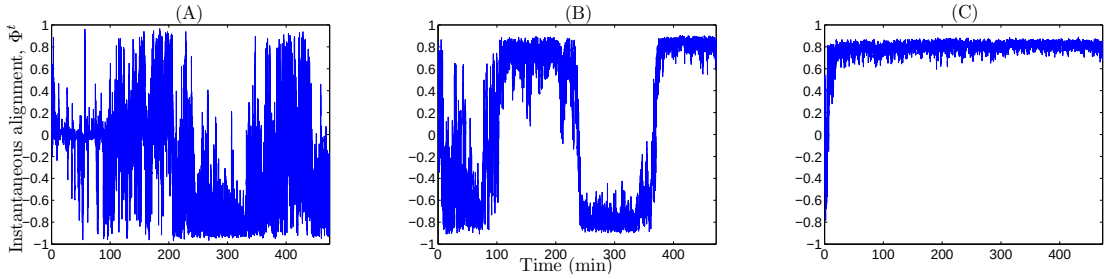


Figure 1.1: *Change in Φ^t over time for three different locust densities. (A) 7 (or 3.47 moving on average), (B) 20 (or 12.05 moving on average), and (C) 60 (or 47.35 moving on average) locusts [4]. These figures were plotted using the codes* `locusts7.m` , `locusts20.m` *and* `locusts60.m` *using original experimental data kindly provided by J. Buhl.*

If locust marching behaviour can be understood and modelled accurately then the consequences may be of great significance. Predictions could be made about the movement of marching bands of locusts and steps taken in order to either control or halt their destructive behaviour.

I aim to start the first segment of the project by simply recreating the dynamics of the above experiment, (see Figure 1.1 (A)-(C)) especially the switching behaviour exhibited in Figure 1.1 (B), using a stochastic differential equation (SDE) for a particle moving in a bistable potential. The properties of the SDE model such as the time it takes for the locusts to switch from one direction to another (mean switching time) and the stationary probability distribution (SPD) of the locust alignment can be found using the backwards Kolmogorov equation and Fokker-Planck (F-P) equation (which I shall derive from first principles) respectively.

It is useful to show that one can qualitatively replicate the behaviour of the experiment in [4] using an SDE and one may even, by changing the parameters of the SDE, be able

to come up with a model which has the same switching time and stationary probability distribution. However, one of the aims of this project is to be able to make predictions using the model. In order to do this I will introduce the one dimensional SPP model of Czirók et al [7] which actually models the locusts as identical individual particles. I will show that by choosing parameters typical of locusts in the field, I will be able to recreate the switching behaviour of the locust alignment, Φ^t, of [4]. This switching behaviour hints that there is an underlying stochastic differential equation modelling the alignment. If this stochastic differential equation could be found then it would be possible to find properties mentioned before such as the mean switching time and the stationary probability distribution.

Fortunately there is a way of doing this using the 'equation-free' technique. This enables the prediction of the defining properties of the underlying SDE using many short-time simulations. In the section where I introduce the equation-free technique I will give comparisons between the equation-free results and long-time simulation results (such as mean switching time and stationary probability distribution) in order to justify the use of such a technique. I will use the technique to find the defining properties (such as the drift, diffusion and potential) of the SDE underlying the alignment's behaviour . I will also modify the technique slightly to allow the same properties to be derived using one long time simulation. I can then apply this to the experimental data of [4] and find the properties of the SDE assumed to be underlying the exhibited switching behaviour (see Figure 1.1 (B)).

While the one dimensional model will be informative, natural locust marching bands move in *two* dimensions. Unfortunately the whole-group instantaneous switching property described above is only apparent when locusts are made to march in an unnatural one dimensional fashion (i.e. in the ring shaped arena of [4]).

In the second segment of the project I will model locusts in two dimensions and take interest in other properties of the model, namely the evolution of certain characteristics of the SPPs. To study these I will employ evolutionary game theory to explain the counter-intuitive results derived from the SPP models and found in nature:

Ever since Darwin made his ideas public the debate to decide at which level natural selection takes place has raged. It was only recently that there was finally a conclusion to this debate and perhaps some may consider it to be counter-intuitive. Surely the species that does the better will win out in a competition between two species and surely the way a species does best is for all the members of that species to work together sacrificing themselves if needs be?

Stotting[2] behaviour in gazelles, for example, reduces the distance between predator and prey and the speed of the pursued prey when performed, and as such increases the risk of being caught and killed by the predator. Originally it was thought to be an altruistic alarm signal to other gazelles in the vicinity, making them aware of an approaching predator. As such the behaviour drove anthropologist Robert Ardrey to conclude that "In such terms [species level selection], and only in such terms, can the Tommie's [Thompson's Gazelle's] alarm signal be explained as the product of evolutionary process."[2]. However, the theories of Smythe [23] enforced by Zahavi [24] gave another interpretation to the stotting behaviour. The idea was that far from being a signal to other gazelles, stotting is really aimed at predators. It is a signal to show the predator that the gazelle is fit and healthy and is fully expecting to outrun him. It also tells the predator that the gazelle

[2]Stotting or pronking is a behaviour of gazelles, particularly Thomson's Gazelles, involving leaping straight upwards before and during pursuit by a predator, typically a cheetah or lion.

is aware of his presence and that any advantage of a surprise attack he might have had has disappeared. Cheetahs, for example, abandon more hunts when the gazelle stots than when it does not, and in the event they do give chase (when the gazelle has previously stotted) they are far less likely to make a kill [5]. In addition, gazelles which are chased, but which outrun the predators, are more likely to stot, and to stot for longer durations, than those which are chased and killed [11]. In their 1988 paper FitzGibbon and Fanshawe conclude that stotting could be an honest signal of a gazelle's ability to outrun predators, which predators take into account when selecting prey [11]. Consequently it advertises to the predator that some of the stotter's neighbouring gazelles who are not stotting are clearly not as fit and healthy as he is. Far from being an altruistic act, it turns out that stotting is selfish, telling the predator to stalk someone else and to leave the stotter alone. This argument could be made more rigorous by using the language of mathematics and applying evolutionary game theory to the situation.

Evolutionary game theory helped to put the last nail in the coffin of the species level selection argument[3] by showing that what is at first counter-intuitive is, often, the only logical solution. Game theory is full of counter-intuitive results, all of which come from making arguments, like the one above, rigorous and following the logic through to its conclusions. I hope to use game theory in this project to explain some of the counter-intuitive results that are derived from the two dimensional SPP models.

To begin the second segment I will outline some of the basics of evolutionary game theory considering intraspecific conflict and competition, leading to the one of the most basic evolutionary games: the 'hawk-dove' game. Next I will explain the game of 'prisoner's dilemma', thought to be prevalent in nature and introduce the two other types of basic evolutionary game. I will go on to define the concepts of evolutionary stable strategies and of Nash equilibria differentiating between pure and mixed strategies (although I will only use pure strategies in my modelling).

Once the relevant background material is in place I will introduce the model itself. I will recreate a model similar to that of Vicsek et al from their paper [26] for SPPs in two dimensions. In this paper Vicsek et al discovered that by varying the density of the particles or the size of the noise (the random perturbation added to the motion of each particle) a transition (phase change) occurred in the particles from disordered movement of individuals to highly aligned collective motion. I aim to recreate this so called 'phase change' by varying another property of the particles: the interaction radius (the range in which a particle will interact with its neighbours). It has been hypothesised, by David Sumpter, that the interaction radius that will be favoured by natural selection will be in the range for which a change in phase occurs. So although there are several properties of the model which it will be interesting to evolve, in order to test this hypothesis, I will evolve the interaction radius of the particles. Using a simple model I aim to apply evolutionary game theory firstly to discover that the evolutionarily stable strategy (ESS) is an interaction radius which is much smaller than expected (thus disproving Sumpter's intuitive hypothesis) and secondly to explain this result. Finding the ESS for the interaction radius will throw light on the possible reasons why natural selection has acted to favour a small interaction radius. This insight will help me to refine my models of locust marching and make them more accurate, thus bringing me back to the main aim of all locust modelling work, that of predicting and halting destructive locust behaviour which affects a large proportion of the

[3] Although today there is still some debate as to which level selection actually takes place it is though to be at the level of the gene. In this project, however, the simulated particles will not have genes and I will only consider varying one characteristic, meaning that selection will be applied at the level of the individual.

world's population.

1.2 Summary of Original Results

What follows is a summary of the main original results in this project set out in order. Segment 1:

1. I will look numerically at how alignment is affected by interaction radius and show that a similar transition, as has already been shown for density and noise [7], [26], occurs (see Sections 3.1 and 5.1).

2. I will test numerically the importance of a weighting parameter, α, to the SPP model and show that in fact its inclusion makes little difference to the results of the model (see Sections 3.2 and 5.1).

3. I will adopt an equation-free approach for the one dimensional SPP model and use it to estimate the drift and diffusion terms for an SDE that describes the evolution of the probability that the SPP model is in a particular state of alignment (see Sections 3.3 and 3.4).

4. I will apply a similar approach to experimental data, again estimating the drift and diffusion terms for a relevant SDE (see Section 3.5).

Segment 2:

1. I will find the size of the optimal radius at which, in the two dimensional SPP model, the particles become aligned with the leader particle (see Section 5.1).

2. I will find the counter-intuitive result that the evolutionarily stable radius, for alignment, appears to be much smaller than the optimal radius (see Section 5.2).

Chapter 2

Stochastic Switching

Stochastic Differential Equations (SDEs) play a prominent role in a range of application areas, including biology, chemistry, epidemiology, mechanics, microelectronics, economics and finance [17] as well as in this project, where SDEs will be used to model the motion of individual animals and the collective motion of groups of animals. I will simulate the SDEs in Matlab, which is an ideal environment given its high level random number generation and graphics facilities.

In this numerical simulation section I will first introduce the idea of Brownian motion and integration with respect to Brownian motion illustrating the difference between, Itô and Stratonovich integrals. After gaining this most basic understanding of SDEs I will go on to describe the Euler-Maruyama numerical method for simulating an SDE. Using this method I will simulate one specific example of a known SDE whose solution will have qualitative resemblance to the average alignment of locusts moving in a sand ring, from the example given in the motivation section above. I will introduce several techniques for analysing the SDE and see how these techniques can be used to analyse a numerical simulation of the behaviour found in [4]. Among the analyses I will carry out will be the derivation of the backwards Kolmogorov and Fokker-Planck equations, the derivation and application of the mean first-passage time and further first-passage time moments and equation-free analysis.

2.1 Brownian Motion

A scalar standard Brownian motion, or standard Wiener process, over $[0, T]$ is a random variable $W(t)$ that depends continuously on $t \in [0, T]$ and satisfies the following three conditions [17]:

1. $W(0) = 0$ (with probability 1).
2. For $0 \leq s < t \leq T$ the random variable given by the increment $W(t) - W(s)$ is normally distributed with mean zero and variance $t-s$; equivalently, $W(t)-W(s) \sim \sqrt{t-s}N(0,1)$, where $N(0,1)$, denotes a normally distributed random variable with zero mean and unit variance.
3. For $0 \leq s < t < u < v \leq T$ the increments $W(t)-W(s)$ and $W(v)-W(u)$ are independent.

For computational purposes it will be useful to consider discretised Brownian motion, where $W(t)$ is specified at discrete time values. Thus set $dt = T/J$ for some positive integer

J and let W_j denote $W(t_j)$ with $t_j = jdt$, for $j = 0, \ldots, J$. Condition (1) says $W_0 = 0$ with probability one. Combining conditions (2) and (3):

$$\begin{aligned} W_j - W_{j-1} &= W(t_j) - W(t_{j-1}) \\ &= \sqrt{t_j - t_{j-1}} N(0,1) \\ &= \sqrt{dt} N(0,1) \\ &= dW_j \quad \text{for} \quad j = 1, 2, \ldots, N, \end{aligned}$$

where each dW_j is an independent random variable of the form $\sqrt{dt}N(0,1)$. This gives the relationship:

$$W_j = W_{j-1} + dW_j,$$

for discretised Brownian motion [17].

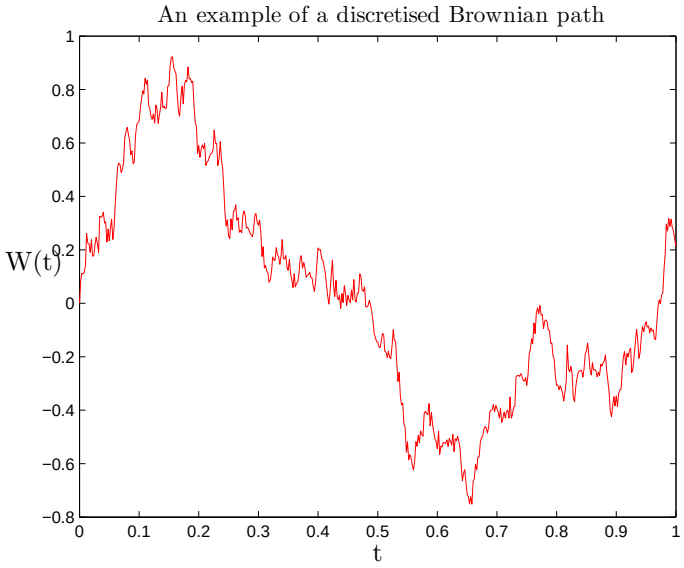


Figure 2.1: *An example of a simple Brownian path with* $dt = 0.002$. *This was calculated and plotted using Matlab code* `BPATH2.m` *[17].*

2.2 Stochastic Integration

Now that I have introduced the concept of a discretised Brownian path, I can introduce the notion of stochastic integrals. Given a suitable deterministic function h, the integral $\int_0^T h(t)dt$ can be approximated by the Riemann sum,

$$\sum_{j=0}^{J-1} h(t_j)(t_{j+1} - t_j), \tag{2.2.1}$$

where the discrete time points are the same as those that were introduced for discretised Brownian motion. This approximation to the integral is often known as the 'left hand

rectangle rule'. In fact the integral can be defined by taking the limit as $dt \to 0$ in (2.2.1). Similarly, consider a sum of the form

$$\sum_{j=0}^{J-1} h(t_j)(W(t_{j+1}) - W(t_j)), \tag{2.2.2}$$

which by analogy with (2.2.1), may be regarded as an approximation to the stochastic integral $\int_0^T h(t)dW(t)$. Here, h is integrated with respect to Brownian motion [17]. An alternative to (2.2.1) is

$$\sum_{j=0}^{J-1} h\left(\frac{t_j + t_{j+1}}{2}\right)(t_{j+1} - t_j), \tag{2.2.3}$$

commonly known as the 'midpoint rectangle rule' which is also a Riemann sum approximation to $\int_0^T h(t)dt$. The corresponding alternative to (2.2.2) is

$$\sum_{j=0}^{J-1} h\left(\frac{t_j + t_{j+1}}{2}\right)(W(t_{j+1}) - W(t_j)). \tag{2.2.4}$$

In the case where $h(t) \equiv W(t)$, the sum (2.2.4) requires $W(t)$ to be evaluated at $t = (t_j + t_{j+1})/2$. It can be shown that adding an independent $N(0, dt/4)$ increment to $(W(t_j) + W(t_{j+1}))/2$, (a trapezium rule type term) gives a value of $W((t_j + t_{j+1})/2)$ that maintains the three conditions for Brownian motion listed earlier and makes the sum easier to evaluate numerically [17].

These two stochastic Riemann sums (2.2.2) and (2.2.4) will give markedly different answers. Even in the limit as $dt \to 0$ this difference does not disappear. This highlights a significant difference between deterministic and stochastic integration: The sums (2.2.1) and (2.2.3) converge to the same limit as $dt \to 0$ independently of the definition of the Riemann sum, whereas, in defining a stochastic integral as the limiting case of a Riemann sum, one must be precise about how the sum is formed. The 'left hand' sum (2.2.2) gives rise to what is known as the Itô integral, whereas the 'midpoint' sum (2.2.4) produces the Stratonovich integral [17]. In what follows the Itô definition of stochastic integration will be used.

2.3 The Euler-Maruyama Method

A scalar autonomous SDE can be written in integral form as

$$X(t) = X_0 + \int_0^t f(X(s))ds + \int_0^t g(X(s))dW(s), \quad 0 \le t \le T. \tag{2.3.1}$$

Here $f(X(s))$ and $g(X(s))$ are scalar functions and the initial condition X_0 is a random variable. The second integral on the right hand side is to be taken with respect to Brownian motion as discussed in the previous section and the Itô version of integration is used. The solution $X(t)$ is a random variable for each t. Rather than defining what it means for $X(t)$ to be a solution of (2.3.1) it is easier to define a numerical method for solving (2.3.1) and regard $X(t)$ as the random variable which arises when the zero step size limit is taken in

the numerical method [17]. It is usual to rewrite (2.3.1) as[1]

$$X(t+dt) - X(t) = dX(t) = f(X(t))dt + g(X(t))dW(t), \quad X(0) = X_0, \quad 0 \leq t \leq T. \tag{2.3.2}$$

If $g \equiv 0$ and X_0 is constant, then the problem becomes deterministic, and (2.3.2) reduces to an ordinary differential equation (ODE) [17].

SDEs can be thought of as defining the motion of a particle moving in a potential $\phi(X(t))$ with a random positional perturbation at each time step, with the solution $X(t)$ representing the position of a particle. In the above SDE, (2.3.2), $f(X(t))$ is known as the drift and $D(X(t)) = g(X(t))^2/2$ is known as the diffusion. The drift and diffusion are related to the potential, $\phi(X(t))$ by the equation $\frac{f(X(t))}{D(X(t))} = -\phi'(X(t))$ where ' denotes differentiation with respect to $X(t)$. $f(X(t))$ is known as the drift because, by its definition, the term involving $f(X(t))$ tends to make the 'particle' *drift* down the gradient of the potential. $D(X(t))$) is known as the diffusion because it is the random term which causes the particle's position to spread out, not just move towards the lowest potential. As mentioned in the paragraph above, this indicates that without the diffusion term an SDE would just become and ODE.

In order to apply a numerical method to (2.3.2) over a time interval $[0, T]$, first discretise the interval. Let $\Delta t = T/J$ for a positive integer J, and $t_j = j\Delta t$. The numerical approximation to $X(t_j)$ will be denoted X_j. Consider the integral form of the SDE over the time period from t_{j-1} to t_j:

$$X(t_j) = X(t_{j-1}) + \int_{t_{j-1}}^{t_j} f(X(s))ds + \int_{t_{j-1}}^{t_j} g(X(s))dW(s). \tag{2.3.3}$$

Approximating all of the terms in (2.3.3) with their numerical counterparts gives the Euler-Maruyama (E-M) method in its usual form [17]:

$$X_j = X_{j-1} + f(X_{j-1})\Delta t + g(X_{j-1})(W(t_j) - W(t_{j-1})), \quad j = 1, \ldots, L \tag{2.3.4}$$

Note that in the deterministic case ($g \equiv 0$ and X_0 is constant) that (2.3.4) reduces to the forward (or explicit) Euler method.

2.4 Applying the Numerical Method to an Example

I used the E-M method to simulate an SDE numerically. In order to replicate the qualitative behaviour of the locusts experiment in [4] (see Figure 1.1 (B) with $X(t)$ representing the average alignment of the particles, Φ^t) I chose a potential that had wells at $x = 1$ and $x = -1$ with a smooth barrier in between the two wells at $x = 0$. This means that the particle should spend some time fluctuating around 1 in the right hand well (without loss of generality) before jumping to the left hand well and fluctuating about -1, then jumping to the right hand well, etc. For simplicity I also chose the diffusion to be constant, $D(X(t)) = 1$ which implies $g(X(t)) = \sqrt{2}$. This means that the relationship between the drift and the potential is $f(X(t)) = -\phi'(X(t))$. The above conditions imply that a possible potential is given by $d\phi(x)/dx = (x-1)(x+1)x = x^3 - x$. By a simple integration $\phi(x) = x^4/4 - x^2/2$, using the arbitrary condition $\phi(0) = 0$ to find the constant of integration to be 0. After a few trial simulations I found that to get an appreciable switching time (average time the particle

[1] It should be noted that one is not allowed to write $dW((t))/dt$, since Brownian motion is nowhere differentiable with probability 1.

stays in one well, a quantity which will be especially useful later on when verifying the validity of some of the analyses undertaken (see Sections 2.7–8)) with noise being chosen from $N(0,1)$ (i.e. with $D(X(t)) = 1$ the time step $\Delta t = 1$ must be chosen) I had to make the potential wells deeper. To do this I multiplied the original potential by a factor of ten so that a particle moving according to equation (2.3.2) would remain longer in each well. The potential (see Figure 2.2) decided upon was[2]

$$\phi(x) = 10(\frac{x^4}{4} - \frac{x^2}{2}). \tag{2.4.1}$$

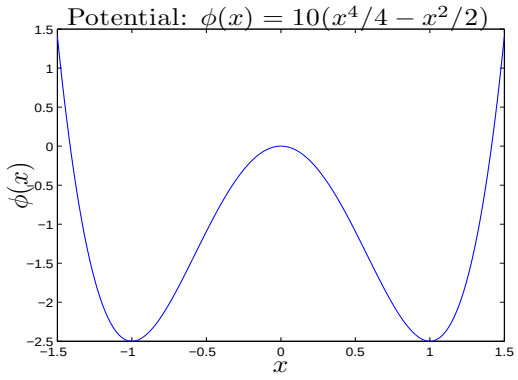


Figure 2.2: *The chosen potential for the SDE (2.3.2):* $\phi(x) = 10(\frac{x^4}{4} - \frac{x^2}{2})$.

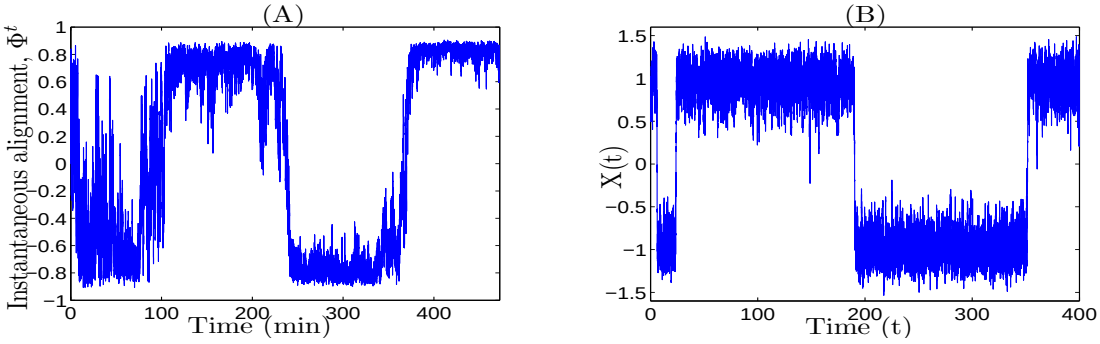


Figure 2.3: *Experimental results (A) compared with the numerical solution of the chosen SDE (B). (Note Figure 1.1 (B) has been renamed (A) in this figure.) The Matlab code used to plot (B) was* `myswitch.m`.

Figure 2.3 (B) is an example of the results of the numerical solution of the stochastic differential equation. (The code used to simulate the SDE is adapted from [17]). The initial condition is given by $X(t) = 1$, representing a situation where all the locusts are travelling in the same positive direction. I have also reproduced the Figure 1.1 (B) so that qualitative comparisons can be drawn. Clearly the noise in the simulation is somewhat

[2]This is often known as a Ginzburg-Landau potential.

larger than in the experiment and in the simulation $X(t)$ can take values larger than 1 which is obviously not possible for the experimental alignment. However, the all important switching behaviour is clearly displayed in both figures.

Now the qualitative similarity has been demonstrated (see Figure 2.3 above) I illustrate techniques which could be used in order to find the important properties of the simulation such as the mean switching time. I also consider the simulation of the SDE as a 'black box'[3]: It is assumed that the drift and diffusion terms of the SDE are unknown. Equation-free analysis can be used to determine these properties which, in turn, will give the underlying potential. Using the following analysis a formula for the mean switching time can be derived. It will be informative to carry out the equation-free analysis on an SDE where the drift and diffusion are known enabling a comparison of the results of the analysis to the actual values of $f(x)$ and $g(x)$. Potentially the equation-free analysis could be used on the locust experiment itself, but it will be practically easier to use on a 1-D numerical model of the experiment to begin with. This way I can find the underlying potential and hence switching time, comparing this theoretical value with a value estimated from stochastic simulation.

2.5 The Fokker-Planck Equation

As in the previous SDE, (2.3.2), consider a situation in which a particle moves in a bistable potential, in other words a potential with two wells. Every time step, dt, the particle updates its position by considering its position at the current time, $x(t)$, adding term which makes it fall back towards the bottom of the well, $f(x(t))$, which is proportional to $-\frac{d\phi(x)}{dx}dt$, and then adding on a random perturbation, $g(x(t))dW(t)$, which consists of a magnitude term $g(x(t))$ and a random term $dW(t) = \sqrt{dt}\xi$, where $\xi \in N(0,1)$ is a scalar, randomly chosen from the normal distribution[4].

At first assume that the functions, $f(X(t))$ and $D(X(t)) = g^2(X(t))/2$, in the stochastic differential equation, are both known:

$$X(t+dt) = X(t) + f(X(t))dt + g(X(t))dW. \tag{2.5.1}$$

Consider the conditional probability distribution $P(x_1, t|x_0, s)$ = "the probability the process is in state x_i at time t, given that at time s it was in state x_0, where $s < t$". The

[3]The term black box refers to a process in which the underlying dynamics are unknown. All that is known about the process is the output. For example in the locust experiment, the underlying dynamics governing the way the locusts move collectively are unknown, but the alignments of the locusts at each time-step are known.

[4]The scaling of the noise term $dW(t) = \sqrt{dt}\xi$ with $\sqrt{dt}$ is important. Clearly it is necessary for $dW(t) \to 0$ as $dt \to 0$, otherwise the particle would not have a definite position at a specific time which means that the problem would not be well defined. Consider two cases: In the first case take $dt = 1$ and in the second case take $dt = \frac{1}{100}$. In a time period equal to one unit of time the particle in the first case will have updated its position once and the corresponding noise term will be taken from the normal distribution, $N(0,1)$. In the same period of time the particle in the second case will have updated its position 100 times. It is important that the noise terms for case 1 and case 2 be of the same size otherwise the stochastic differential equation will be dependent on the time step. The noise term for the second case will be from a distribution $\sqrt{\frac{1}{100}}N_1(0,1) + \sqrt{\frac{1}{100}}N_2(0,1) + \ldots + \sqrt{\frac{1}{100}}N_{100}(0,1) = \sqrt{\frac{1}{100}}\sum_{i=1}^{100} N_i(0,1)$. By a property of normal distributions this new distribution is equal to $N(0,1)$. However, if the noise had not been scaled with $\sqrt{dt}$ then the variance of this distribution would not have been 1 and there would be an inconsistency.

stochastic differential equation (2.5.1) satisfies the Markov property [14] :

$$P(X(t_n), t_n | X(t_0), t_0, X(t_1), t_1, \ldots, X(t_{n-1}), t_{n-1}) = P(X(t_n), t_n | X(t_{n-1}), t_{n-1}) \text{ for any } t_0 < t_1 < \ldots < t_n.$$

Informally, the Markov property says that given the past history of the process, future behaviour depends only on the current state: Given that $X(t') = y$ then the ability to predict $X(t)$ for any time $t > t'$ will not be enhanced by any knowledge of the process earlier than t'. Any stochastic process that has this 'past forgetting' property is a Markovian stochastic process or Markov process [14]. For the SDE (2.5.1) it would be expected that given the initial conditions $y = -1$ at $s = 0$, without loss of generality, that the probability distribution would be bimodal with peaks over the two potential wells. The fact that this distribution is expected reflects the fact that after a long time the simulation 'forgets' where it started. After a long time the probability distribution is said to converge to a stationary distribution i.e. a probability distribution that does not depend on time. The Fokker-Planck (F-P) equation can be used to find the precise formula of the stationary probability distribution (SPD).

First consider the continuous Chapman-Kolmogorov (C-K) equation:

$$P(x, t + dt | y, s) = \int_{\mathbb{R}} P(x, t + dt | z, t) P(z, t | y, s) dz. \tag{2.5.2}$$

Intuitively this equation makes sense: The probability of being at x at time $t + dt$ (where dt is a small increment), starting at y at time s, is equal to the 'sum' of all the probabilities of going from y to some intermediate $z \in \mathbb{R}$ from time s to time t and then from z to x in time dt for all possible z. Since z is continuous not discrete this 'sum' of probabilities is actually an integral. A formal proof of the C-K equation is given in [14] (page 62), but I shall omit it here.

In order to proceed I need to make clear the definition of a test function. $\psi(x)$ is said to be a test function [20] if:

1. $\psi(x)$ is a C^∞ function. That is, it has derivatives of all orders at each point $x \in \mathbb{R}$.
2. $\psi(x)$ has *compact support*. That is, it vanishes outside some interval (a, b). (The support is the closure of the set where ψ is nonzero.)

This first property makes test functions very smooth indeed, which ensures that if $\psi(x)$ is a test function then so are all its derivatives.

Multiplying the C-K equation (2.5.2) by a test function $\psi(x)$ and integrating over the whole of the real line with respect to x gives:

$$\int_{\mathbb{R}} \psi(x) P(x, t + dt | y, s) dx = \int_{\mathbb{R}} \int_{\mathbb{R}} \psi(x) P(x, t + dt | z, t) P(z, t | y, s) dz dx. \tag{2.5.3}$$

Consider the right hand side (RHS) of equation (2.5.3). Take $P(z, t|y, s)$ out of the integral with respect to x using Fubini's theorem to give,

$$\text{RHS} = \int_{\mathbb{R}} P(z, t | y, s) \int_{\mathbb{R}} \psi(x) P(x, t + dt | z, t) dx dz. \tag{2.5.4}$$

Expand $\psi(x)$ in a Taylor series around z

$$\psi(x) = \psi(z) + (x - z)\psi'(z) + \frac{(x - z)^2}{2} \psi''(z) + O((x - z)^3). \tag{2.5.5}$$

Substituting the above formula for $\psi(x)$ into (2.5.4) and using distributivity, split the RHS into three separate integrals which will be numbered (1), (2) and (3):

$$(1) = \int_{\mathbb{R}} P(z,t|y,s)\psi(z)\left\{\int_{\mathbb{R}} P(x,t+dt|z,t)dx\right\}dz = \int_{\mathbb{R}} \psi(z)P(z,t|y,s)dz. \tag{2.5.6}$$

The second equality holds since the integral in the curly braces represents the probability of starting in state z at time t and being in state x by time $t+dt$ for any $x \in \mathbb{R}$, which is clearly equal to one as the process is bound to go somewhere in time dt.

$$\begin{aligned}(2) &= \int_{\mathbb{R}} P(z,t|y,s)\frac{d\psi(z)}{dz}\left\{\int_{\mathbb{R}}(x-z)P(x,t+dt|z,t)dx\right\}dz \\ &= -\int_{\mathbb{R}} \psi(z)\frac{\partial}{\partial z}\left\{P(z,t|y,s)\int_{\mathbb{R}}(x-z)P(x,t+dt|z,t)dx\right\}dz. \end{aligned}\tag{2.5.7}$$

The second equality follows from using integration by parts and property 2. (compact support) of the test function $\psi(x)$.

Thus far the SDE has not been used in the derivation of the F-P equation. Recall that z is the state of the random variable, X, at time t and x is the state of the random variable time dt later. Equation (2.5.1) implies,

$$x - z = X(t+dt) - X(t) = f(X(t))dt + g(X(t))dW = f(z)dt + g(z)dW, \tag{2.5.8}$$

and substituting this into (2.5.7) gives,

$$(2) = -\int_{\mathbb{R}} \psi(z)\frac{\partial}{\partial z}\left\{P(z,t|y,s)\int_{\mathbb{R}}(f(z)dt + g(z)dW)P(x,t+dt|z,t)dx\right\}dz. \tag{2.5.9}$$

The second integral in (2.5.9) is the expectation of $f(z)dt + g(z)dW$, but, since the noise term dW is from a normal distribution, the expectation of the second term is zero so it vanishes. From the remaining terms $f(z)dt$ can be taken out of the integral in x leaving $\int_{\mathbb{R}} P(x,t+dt|z,t)dx = 1$ as before. This implies,

$$(2) = -\int_{\mathbb{R}} \psi(z)\frac{\partial}{\partial z}\left\{P(z,t|y,s)f(z)dt)\right\}dz. \tag{2.5.10}$$

The third integral is acted on by a double integration by parts to give:

$$\begin{aligned}(3) &= \int_{\mathbb{R}} P(z,t|y,s)\frac{d^2\psi(z)}{dz^2}\left\{\int_{\mathbb{R}}\frac{(x-z)^2}{2}P(x,t+dt|z,t)dx\right\}dz \\ &= \int_{\mathbb{R}} \psi(z)\frac{\partial^2}{\partial z^2}\left\{P(z,t|y,s)\int_{\mathbb{R}}\frac{(x-z)^2}{2}P(x,t+dt|z,t)dx\right\}dz. \end{aligned}\tag{2.5.11}$$

Again the properties of $\psi(z)'$ and $\psi(z)$ as test functions are used. This time use SDE (2.5.1) to consider

$$\begin{aligned}(x-z)^2 &= (X(t+dt)-X(t))^2 = [f(X(t))dt + g(X(t))dW]^2 \\ &= f(X(t))^2dt^2 + 2f(X(t))g(X(t))dWdt + g(X(t))^2dW^2 \\ &= f(z)^2dt^2 + 2f(z)g(z)dWdt + g(z)^2dW^2. \end{aligned}\tag{2.5.12}$$

The second term in (2.5.12) vanishes, when substituted into (2.5.11) for the same reasons as in case (2). The first term is multiplied by dt^2 and dt is small, so the first term is quadratically small and hence is also neglected. The third term is all that remains. Again using the idea of an expectation, since g is taken to be constant, $E(g^2) = g^2$, and since dW is normally distributed:

$$\mathrm{E}(dW^2) = dt\mathrm{E}((N(0,1))^2) = dt[\mathrm{Var}(N(0,1)) + (\mathrm{E}(N(0,1)))^2] = dt\mathrm{Var}(N(0,1)) = dt \tag{2.5.13}$$

Substituting these results back into (2.5.11) and tidying up as before implies

$$(3) = \int_{\mathbb{R}} \psi(z) \frac{\partial^2}{\partial z^2} \left\{ P(z,t|y,s) \frac{g(z)^2}{2} dt) \right\} dz. \tag{2.5.14}$$

Now bringing back together integrals (1), (2) and (3) from equations (2.5.6), (2.5.10) and (2.5.14) respectively,

$$RHS = \int_{\mathbb{R}} \psi(z) \left\{ P(z,t|y,s) - \frac{\partial}{\partial z}[P(z,t|y,s)f(z)dt] + \frac{\partial^2}{\partial z^2}\left[P(z,t|y,s)\frac{g(z)^2}{2}dt \right] \right\} dz. \tag{2.5.15}$$

Equation (2.5.3) can now be rewritten as

$$\int_{\mathbb{R}} \psi(z) \left\{ P(z,t+dt|y,s) - P(z,t|y,s) + \frac{\partial}{\partial z}[P(z,t|y,s)f(z)dt] - \frac{\partial^2}{\partial z^2}\left[P(z,t|y,s)\frac{g(z)^2}{2}dt \right] \right\} dz = 0. \tag{2.5.16}$$

Using the fact that $\psi(z)$ is an arbitrary test function

$$P(z,t+dt|y,s) - P(z,t|y,s) + \frac{\partial}{\partial z}[P(z,t|y,s)f(z)dt] - \frac{\partial^2}{\partial z^2}\left[P(z,t|y,s)\frac{g(z)^2}{2}dt \right] = 0. \tag{2.5.17}$$

Dividing through by dt and taking the limit as $dt \to 0$ we finally arrive at the (Itô) Fokker-Planck equation[5]:

$$\frac{\partial P(z,t|y,s)}{\partial t} = -\frac{\partial}{\partial z}\left(P(z,t|y,s)f(z)\right) + \frac{\partial^2}{\partial z^2}\left(\frac{g(z)^2 P(z,t|y,s)}{2}\right). \tag{2.5.18}$$

Given the initial condition $x(0) = -1$, this translates as an initial condition for the F-P equation: $P(z,0|-1,0) = \delta_z(-1)$, where $\delta_z(-1)$ denotes the Dirac delta in the variable z focussed at $z = -1$.

2.6 Stationary Probability Distribution

As mentioned before since the SDE is Markovian, after a long time the process essentially 'forgets' where it started. This means that the probability distribution after a long time should be a fixed curve and in the case of the two-welled potential a bimodal distribution is expected. This so called 'stationary distribution', $P_s(z)$, is time independent and the F-P

[5]Using the Stratonovich version of stochastic integration the F-P equation derived is slightly different [25].

equation (2.5.18) can be used to calculate it. Since the SPD is time independent $\left(\frac{\partial P_s(z)}{\partial t} = 0\right)$ the F-P equation becomes:

$$\frac{\partial}{\partial z}\left(P_s(z)f(z)\right) = \frac{\partial^2}{\partial z^2}\left(\frac{g(z)^2 P_s(z)}{2}\right) = \frac{\partial^2}{\partial z^2}\left(D(z)P_s(z)\right). \tag{2.6.1}$$

It has already been decided that in this specific SDE the diffusion term will be constant, (specifically $D = 1$), but for the sake of generality I will leave the diffusion term, $D(z)$, in the analysis and apply the consequences of it being constant later. In this case (2.6.1) can be integrated once with respect to z taking the constant of integration to be zero (assuming that there are no sources or sinks of probability):

$$P_s(z)f(z) = \frac{\partial(P_s(z)D(z))}{\partial z}, \tag{2.6.2}$$

$$\text{which implies } P_s(z)\left\{\frac{f(z) - D'(z)}{D(z)}\right\} = \frac{\partial P_s(z)}{\partial z}. \tag{2.6.3}$$

We can solve (2.6.3) using separation of variables as

$$P_s(z) = C\exp\left\{\int_0^z \frac{f(s)}{D(s)}ds - \ln(D(z))\right\}. \tag{2.6.4}$$

Since this is a probability distribution its integral, over all space, must be one[6]. The distribution must be normalised by choosing C such that

$$C^{-1} = \int_{\mathbb{R}} \exp\left\{\int_0^z \frac{f(s)}{D(s)}ds - \ln(D(z))\right\}dz. \tag{2.6.5}$$

This is how the equation for the potential of the stochastic differential equation is derived. The potential is defined as the negative of the exponent in the equation for the SPD (2.6.4):

$$\tilde{\phi}(z) = -\int_0^z \frac{f(s)}{D(s)}ds + \ln(D(z)) \tag{2.6.6}$$

This is not the same as the equation for the potential, ϕ, given in Section 2.3. However, if $D(z)$ is constant, $\exp(\ln(D)) = D$ is consequently absorbed into the normalising constant C and the potential becomes

$$\phi(z) = -\int_0^z \frac{f(s)}{D}ds$$

$$\text{which implies } \phi'(z) = -\frac{f(z)}{D}. \tag{2.6.7}$$

Continue to assume D is constant and substitute for $\frac{f(z)}{D}$ (using (2.6.7)) in (2.6.2). The resulting equation is

$$\frac{dP_s(z)}{dz} = -\phi'(z)P_s(z), \tag{2.6.8}$$

[6]Here I have assumed that a stationary probability distribution exists. A way to test this is to find the normalising constant, C. If $C = 0$ or ∞ then the probability distribution does not exist.

which can be solved to give the SPD,

$$P_s(z) = \frac{\exp\left[-\phi(z)\right]}{\int_{\mathbb{R}} \exp\left[-\phi(z)\right]} dz, \tag{2.6.9}$$

as expected. For the specific potential chosen earlier (equation 2.4.1) the SPD is given by the equation

$$P_s(z) = \frac{\exp\left[-10(x^4/4 - x^2/2)\right]}{\int_{\mathbb{R}} \exp\left[-10(x^4/4 - x^2/2)\right]}. \tag{2.6.10}$$

In order to verify this equation numerically I ran the stochastic simulation of the SDE for a long time, recording the position of the particle at regular intervals (every 50 time-steps). These values of position were then plotted in a histogram to give a diagram of an approximate probability distribution (see Figure 2.4).

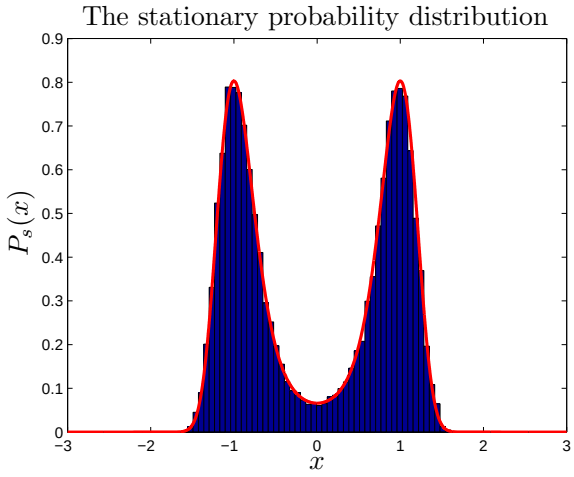


Figure 2.4: *Two methods of finding the SPD. The red line represents the equation of the SPD (2.6.10) derived from the F-P equation. The histogram represents the numerical approximation to the SPD from the codes* `myswitchprob.m` *and* `stationaryprobability.m`*. It is clear from this figure that the F-P equation is correct in the prediction of the SPD as it matches the numerical simulation of the SDE well.*

2.7 Moments of the First Passage Time

An important property of an SDE with a bistable potential is the mean switching time or the mean first-passage time: the average time it takes for a particle to switch between potential wells. In the locust problem which originally motivated the model, the mean switching time represents the average time taken for the alignment of the locusts to go from positive to negative. We can use the backwards Kolmogorov equation (2.7.4) to derive the equation for the mean of the first-passage time and higher moments of the first-passage time[7].

[7]Throughout the analysis it will be assumed that the potential barrier (i.e. the value of x which is considered to be the barrier between the two states and which is crossed when a 'switch' occurs) will be at $x = 0$ without loss of generality. The analysis could be carried out with a potential barrier at a general position $x = x_b$ for example.

Recall that the general single variable F-P equation can be written:

$$\frac{\partial P(x,t)}{\partial t} = -\frac{\partial (f(x)P(x,t))}{\partial x} + \frac{\partial^2 (D(x)P(x,t))}{\partial x^2}, \tag{2.7.1}$$

where, as before, $f(x)$ is the drift and $D(x)$ is the diffusion coefficient ($D(x) = g(x)^2/2$). Although in the specific SDE example D is taken to be constant, in this general derivation I allow D to be a function of x. The steady state solution (2.6.4) is given by

$$P_s = \frac{\exp\left[\int_{-\infty}^{x} \frac{f(x)}{D(x)}\right] dx}{D(x) \int_{-\infty}^{\infty} \frac{1}{D(x)} \exp\left[\int_{-\infty}^{x} \frac{f(x)}{D(x)}\right] dx}, \tag{2.7.2}$$

where the limits of the integral should be thought of as a limit

$$\text{“} \int_{-\infty}^{\infty} dx = \lim_{R\to\infty} \int_{R}^{R} dx \text{”}, \tag{2.7.3}$$

especially when $\phi(x)$ satisfies

$$\lim_{x\to\pm\infty} \phi(x) = \infty,$$

as it does in the example SDE[8].

In order to find the moments of the first passage time I will need to consider Kolmogorov's backwards equation[9] [13], the adjoint of the F-P equation (2.7.1):

$$\frac{\partial P}{\partial t}(y,t|x,s) = f(x)\frac{\partial P}{\partial x}(y,t|x,s) + D(x)\frac{\partial^2 P}{\partial x^2}(y,t|x,s) \tag{2.7.4}$$

Given that a process starts at $x_0 \in (-\infty, 0)$ at time $t = 0$, the probability that it is in the interval $(-\infty, 0)$ at time t is given by

$$G(x_0,t) = \int_{-\infty}^{0} P(y,t|x,0)dy. \tag{2.7.5}$$

Integrate (2.7.4) between $-\infty$ and 0, with respect to y, and use the fact that x is independent of y to take the derivatives outside the integrals. Equation (2.7.4) becomes

$$\frac{\partial G}{\partial t} = f(x)\frac{\partial G}{\partial x} + D(x)\frac{\partial^2 G}{\partial x^2}. \tag{2.7.6}$$

To solve a PDE of this sort, uniquely, one initial condition and two boundary conditions are required. The initial condition is [14],

$$G(x_0, 0) = 1.$$

This simply implies that the initial point x_0 lies in $(-\infty, 0)$, which has already been assumed to be true. Depending on the situation the boundary conditions used can be a mix of absorbing and reflecting or just absorbing, but clearly they can not both be reflecting boundary conditions as the process would never leave the region and the switching time

[8] In the case $D(x)$ = constant the $\frac{1}{D(x)}$ in the numerator and the denominator of (2.7.2) would cancel, but here $D(x)$ is considered to be a function of x, so $\frac{1}{D(x)}$ must remain in the formula.

[9] Its derivation is similar to that of the F-P equation and as such I have included it as Appendix A.

would be infinite. In the case of the double welled potential, the boundary condition at $x = \infty$ will be reflecting and the boundary condition at $x = 0$ will be absorbing. This means that the process can only leave by $x = 0$. The boundary condition at $x = -\infty$ will be

$$G'(-\infty, t) = 0,$$

where $'$ denotes differentiation with respect to x. This implies that $G(-\infty + \varepsilon, t) = G(\infty, t)$ for all infinitesimally small $\varepsilon > 0$; hence if x_0 is taken very close to $-\infty$ then the probability of x being in $(-\infty, 0)$ for any $t > 0$ is not reduced if x_0 is taken even closer to $-\infty$. This means that x can not exit the interval at $-\infty$, which implies that the boundary condition is reflective. The other boundary condition at $x = 0$ must be:

$$G(0, t) = 0.$$

This boundary condition implies that if $x_0 = 0$ then the process will not be inside $(\infty, 0)$ for anytime $t > 0$; hence because the process is markovian and therefore temporally homogeneous if $x = 0$ for any t' then x will not be inside $(\infty, 0)$ for $t > t'$. This implies that the boundary condition is absorbing [14].

Let the time that the process leaves $(-\infty, 0)$ be called T. For small dt, the probability that the variable leaves $(-\infty, 0)$ between t and $t + dt$ is given by

$$G(x, t) - G(x, t + dt) = -\frac{\partial G(x, t)}{\partial t} dt + O(dt). \tag{2.7.7}$$

Therefore the average of any function of T, $h(T)$, is expressible as

$$\begin{aligned} \langle h(T) \rangle &= -\int_0^\infty h(t) \frac{\partial G(x, t)}{\partial t} dt \\ &= -[h(t)G(x, t)]_0^\infty + \int_0^\infty \frac{dh(t)}{dt} G(x, t) dt \\ &= h(0) + \int_0^\infty \frac{dh(t)}{dt} G(x, t) dt \qquad \text{for } x < 0, \end{aligned} \tag{2.7.8}$$

using (for the third equality) the further condition $G(x, \infty) = 0$ (which represents the fact that after infinite time the process is bound to have jumped over the potential barrier) and the initial condition, $G(x, 0) = 1$ [14]. Consequently the mean first-passage time (i.e. $h(T) = T$) is

$$T(x) = \langle T(x) \rangle = \int_0^\infty G(x, t) dt, \tag{2.7.9}$$

starting from $x \in (-\infty, 0)$ at $t = 0$. Combining equations (2.7.6) and (2.7.9) by integrating both sides of (2.7.6) between 0 and ∞ with respect to t and using the initial condition and the condition $G(x, \infty) = 0$ gives the equation for the mean first-passage time:

$$f(x) \frac{\partial T}{\partial x} + D(x) \frac{\partial^2 T}{dx^2} = -1 \tag{2.7.10}$$

Let $\eta \equiv T'$. Then η satisfies

$$f\eta + D\eta' = -1,$$

or equivalently,

$$\eta' = -\frac{f}{D}\eta - \frac{1}{D}. \tag{2.7.11}$$

Solving (2.7.11) for η gives,

$$\eta(x) = \exp\left[-\int_{-\infty}^{x} \frac{f(y)}{D(y)}dy\right] A - \int_{-\infty}^{x} \exp\left[-\int_{y}^{x} \frac{f(z)}{D(z)}dz\right] \frac{1}{D(y)}dy, \tag{2.7.12}$$

where A is an as yet undefined constant. Again these integrals should be interpreted in the same sense as described in (2.7.3) [13]. For boundaries such as $x = -\infty$ where $\phi(-\infty) = \infty$ the reflecting boundary condition can be expressed as $T'(-\infty) = \eta(-\infty) = 0$ [13]. Using this boundary condition, equation (2.7.12) implies $A = 0$ and hence

$$\eta(x) = -\int_{-\infty}^{x} \exp\left[-\int_{y}^{x} \frac{f(z)}{D(z)}dz\right] \frac{1}{D(y)}dy. \tag{2.7.13}$$

For notational convenience introduce

$$\beta(x) \equiv \exp\left[\int_{0}^{x} \frac{f(y)}{D(y)}dy\right]. \tag{2.7.14}$$

Using this notation and integrating (2.7.13) the solution to (2.7.10) can be written as

$$T(x) = B - \int_{0}^{x} \int_{-\infty}^{y} \frac{\beta(z)}{\beta(y)} \frac{1}{D(z)}dzdy. \tag{2.7.15}$$

B is determined using the consequence of the absorbing boundary condition, $T(0) = 0$, which clearly implies $B = 0$. Therefore the equation for the mean first passage time is[10],

$$T(x) = \int_{x}^{0} \int_{-\infty}^{y} \frac{\beta(z)}{\beta(y)} \frac{1}{D(z)}dzdy. \tag{2.7.16}$$

It should also be noted that in the new notation of (2.7.14)

$$P_s(x) = \frac{\beta(x)/D(x)}{\int_{\mathbb{R}} \beta(y)/D(y)dy}, \tag{2.7.17}$$

which when substituted into (2.7.16) gives an equivalent form for $T(x)$,

$$T(x) = \int_{x}^{0} \frac{1}{D(y)P_s(y)} \int_{-\infty}^{y} P_s(z)dzdy.$$

Having calculated a formula for the mean first-passage time the entire first-passage time distribution can now be calculated [13]. Define $T_n(x)$, the nth moment of switching time by,

$$T_n(x) = \langle T^n \rangle = n \int_{0}^{\infty} t^{n-1} G(x,t) \quad \text{for} \quad n > 0. \tag{2.7.18}$$

From (2.7.8)

$$T_0(x) = \langle T^0 \rangle = \langle 1 \rangle = 1 + \int_{0}^{\infty} \frac{d1}{dt} G(x,t)dt = 1. \tag{2.7.19}$$

[10]It should be recalled that for the SDE (2.5.1) $D(x)$ was chosen to be constant, so the formula (2.7.16) simplifies significantly.

If both sides of (2.7.6) are multiplied by t^{n-1} and integrated with respect to t and subsequently multiplied by n, it gives

$$\begin{aligned} f(x)\frac{\partial T_n}{\partial x} + D(x)\frac{\partial^2 T_n}{\partial x^2} &= n\int_0^\infty t^{n-1}\frac{\partial G(x,t)}{\partial t}dt \\ &= n[t^{n-1}G(x,t)]_0^\infty - n(n-1)\int_0^\infty t^{n-2}G(x,t)dt \\ &= -nT_{n-1}, \end{aligned} \tag{2.7.20}$$

where the third equality follows from the condition $G(x,\infty) = 0$ for all x. This is a recurrence relation for T_n with boundary conditions $T_n(0) = 0$ and $T_n'(-\infty) = 0$. This recursion relation can be made simpler by means of Fourier transforms, but the analysis is omitted here (see [13]). Using this recursion relation as many moments of the first-passage time as are necessary can be calculated. However, the most useful moment will be the first, giving the mean first-passage time.

2.8 Mean Switching Times

Recall that for the example SDE, (2.5.1), $D(x)$ is considered to be constant and $f(x)/D(x) = -\phi'(x) = -10(x^3 - x)$. The formula for the mean first passage time or mean switching time given in (2.7.16) simplifies significantly.

First consider $\beta(x)$ as defined in (2.7.14) and substitute in for $\frac{f(y)}{D(y)} = -\phi'(y)$ remembering that $D(y) = D$ is constant:

$$\beta(x) = \exp\left[\int_0^x \frac{f(y)}{D(y)}dy\right] = \exp\left[\int_0^x -\phi'(y)dy\right] = \exp\left[-\phi(x)\right]\exp\left[\phi(0)\right] \tag{2.8.1}$$

Substituting formula (2.8.1) for $\beta(x)$ into equation (2.7.16) gives

$$T(x) = \frac{1}{D}\int_x^0 \int_{-\infty}^y \frac{\exp\left[\phi(y)\right]\exp\left[\phi(0)\right]}{\exp\left[\phi(z)\right]\exp\left[\phi(0)\right]}dzdy. \tag{2.8.2}$$

The $\exp\left[\phi(0)\right]$ terms cancel leaving,

$$T(x) = \frac{1}{D}\int_x^0 \exp\left[\phi(y)\right]\int_{-\infty}^y \exp\left[-\phi(z)\right]dzdy. \tag{2.8.3}$$

The x coordinate of the stationary point to the left of the potential barrier is denoted x_m the one on the right of the potential barrier is denoted x_M and the position of barrier itself is denoted x_b (in what follows I will use the more general x_b to denote the potential barrier as opposed to the specific example $x_b = 0$ used earlier). The generally accepted measure of mean switching time is to find how long it takes the process to reach x_b given that it starts at x_m. Given the chosen potential, the initial condition is $x_m = -1$ and therefore, the mean switching time is $T(x_m) = T(-1)$:

$$T(x_m) = \int_{x_m}^{x_b} \exp\left[\phi(y)\right]\int_{-\infty}^y \frac{1}{D}\exp\left[-\phi(z)\right]dzdy. \tag{2.8.4}$$

Equation (2.8.4) can be simplified if the height of the potential barrier ($\phi(-1) - \phi(0) = 2.5$ in our case) is large compared to the noise strength. If this is the case then almost all of the weight of the function $\exp\left[-\phi(z)\right]$ is located at $z = x_m$. This implies that the inner integral is essentially constant for $x_m < x < x_b$. Therefore the limit y in this integral can be replaced by x_b, allowing the two integrals to be evaluated separately [10]:

$$T(x_m) = \int_{x_m}^{x_b} \exp\left[\phi(y)\right] dy \int_{-\infty}^{x_b} \frac{1}{D} \exp\left[-\phi(y)\right] dy. \tag{2.8.5}$$

The main contribution from the first integral comes from the region around x_b and the main contribution from the second integral comes from the region around x_m. Consequently, expanding $\phi(x)$, using Taylor series

$$\phi(x) \approx \phi(x_b) - \frac{1}{2}|\phi''(x_b)|(x - x_b)^2,$$
$$\phi(x) \approx \phi(x_m) + \frac{1}{2}\phi''(x_m)(x - x_m)^2,$$

for the first and second integrals respectively [10]. When these expansions are used in equation (2.8.5) the following approximate result is obtained:

$$T(x_m) = \frac{4\pi \exp[\frac{\phi(x_b)-\phi(x_m)}{D}]}{2\sqrt{\phi''(x_m)|\phi''(x_b)|}} \tag{2.8.6}$$

Substituting $x_m = -1$ and chosen potential $\phi(y) = 10(y^4/4 - y^2/2)$ into (2.8.4–6) gives equations for the mean switching time for the specific example which can be evaluated numerically:

$$\begin{aligned}
T_{exact}(-1) &= \int_{-1}^{0} \exp\left[10(y^4/4 - y^2/2)\right] \int_{-\infty}^{y} \frac{1}{D} \exp\left[-10(z^4/4 - z^2/2)\right] dz dy, \\
T_{approx1}(-1) &= \int_{-1}^{0} \exp\left[10(y^4/4 - y^2/2)\right] dy \int_{-\infty}^{0} \frac{1}{D} \exp\left[-10(y^4/4 - y^2/2)\right] dy, \\
T_{approx2}(-1) &= \frac{4\pi \exp[2.5/D]}{2\sqrt{20|-10|}} = \frac{4\pi \exp[2.5/D]}{2\sqrt{200}}.
\end{aligned}$$

I used the Matlab code `switchingtimes.m` to evaluate the above formulae for the switching time. I also used the Fortran code `switch.f90` to evaluate the mean switching time using repeated simulations of the stochastic differential equation. This was done by having the initial state of the SDE at the point where the potential is minimised and applying the stochastic update equation (2.2.3) repeatedly until the state of the stochastic differential equation reached zero, the value of the potential barrier for the given potential. This was done 100,000 times and the results averaged to find an approximation to the mean switching time. The results are as given in Table 2.1 below:

Table 2.1 obviously illustrates the close relationship between the first three methods. The many-repeat average formula gives approximately the same answer as the exact formula. Possible reasons for the small discrepancy are that the numerical integration carried out to find the exact formula may not be accurate enough, or that an insufficient number of realisations were made when the many-repeat average was found.

Method of Evaluation	Mean Switching Time (3 d.p.)
Average over 100,000 repeats	3.087
Exact formula (2.8.4)	3.082
First approximation (2.8.5)	3.313
Second approximation (2.8.6)	5.413

Table 2.1: *Mean switching time evaluated using four different methods.*

It can also be seen that the first approximation to the exact integral gives a good approximation to the exact formula for this choice of SDE with a larger discrepancy with the experimentally measured value than the exact formula gives, as expected. The second approximation is a poor approximation to the exact formula. However, it is at least of the same order of magnitude as the exact formula. This formula could be of use if one only needs to know the order of magnitude of the switching time and does not want to spend time doing a lengthy numerical integration. These results reinforce the accuracy of both the experimental SDE code and of the reliability of the theory underpinning the F-P equation and the derived formulae for the mean switching time.

2.9 Equation-Free Analysis

Often it will be the case that although it is expected that a process is modelled by an SDE of the form (2.3.2) the drift and diffusion terms are unknown so an accurate quantitative model of the behaviour cannot be created. For example in the locust experiment [4] it is expected that the behaviour of the alignment[11] at time t, $X(t)$, can be modelled by an equation of the form (2.3.2):

$$X(t+dt) - X(t) = f(X(t))dt + g(X(t))dW(t), \quad 0 \leq t \leq T. \tag{2.9.1}$$

This expectation comes from the qualitative similarity of the switching behaviour of the experimental results and such an SDE, whose underlying drift and diffusion terms are not known (see Figure 2.3 on page 10). This is where equation-free methods come in.

To find the drift term, f, use the idea that the mean of the second term on the right of (2.9.1), gdW, is zero since $dW \sim N(0,1)$ and the mean of $N(0,1)$ is zero. This means that $f(x)$ can be found as

$$f(X) = \lim_{\delta t \to 0} \left\langle \frac{X(t+\delta t) - X(t)}{\delta t} \right\rangle, \tag{2.9.2}$$

where $\langle\rangle$ represents the average over all the repeats of the simulation and δt is a small number of time steps of the process. In order to find f on the region (a,b) for example, where $a, b \in \mathbb{R}$, split (a,b) into a grid of N equally space points. Start the simulation at each grid point and run the simulation for a very short time δt (where, for convenience, δt is some scalar multiple of the numerical time step dt) then record $x(t+\delta t)$. Do this a large number of times[12] and take the average of the recorded values of $x(t+\delta t)$ for each grid point.

[11] Previously in Section 1.1 alignment was denoted Φ^t but for convenience of further working we shall use $X(t)$

[12] For the example in this project 100 repeats at each grid point should be enough to eliminate the term containing g.

It is possible to compute D in a similar to manner to f. Consider (2.9.1); squaring both sides gives

$$\begin{aligned}[X(t+\delta t)-X(t)]^2 &= [f\delta t + gdW]^2 \\ &= f^2\delta t^2 + 2fgdW\delta t + g^2dW^2. \\ &= f^2\delta t^2 + 2fgdW\delta t + 2DdW^2.\end{aligned}$$

Again split the region (a, b), where D is to be found, into a grid of N equally space points. For each grid point run the simulation for a short time δt for a large number of repeats, and calculate:

$$\left\langle [X(t+\delta t)-X(t)]^2 \right\rangle = \langle f^2\rangle\delta t^2 + 2\langle fgdW\rangle\delta t + \langle 2DdW^2\rangle. \tag{2.9.3}$$

The right hand side of (2.9.3) reduces to $2D\delta t$ since the quadratically small term in δt is neglected and the middle term vanishes since its mean is zero. Since $dW \sim \sqrt{\delta t}N(0,1)$ the mean of its square is equal to its variance (since its mean is zero) which is equal to δt. Therefore,

$$2D = g(X)^2 = \lim_{\delta t\to 0}\left\langle \frac{[X(t+\delta t)-X(t)]^2}{\delta t}\right\rangle. \tag{2.9.4}$$

The choice of δt is important when it comes to the accuracy of finding f and D. Although any reasonable choice of δt i.e. $\delta t < 1$ will give an approximation to f and D it turns out that the smaller (nonzero) δt is, the better the approximation to D and the worse the approximation to f is. The opposite is true with larger δt. The reason for this is that, although both the formulae for f and D are true in the limit as $\delta t \to 0$, when approximating numerically this limit cannot actually be taken. The best one can do is to consider small values of δt. The scaling of the two terms becomes important as the size of δt is varied. Since δt is a scalar multiple of dt it is found that for large δt, dt is large and hence the dominant term in the stochastic differential equation (2.3.2) is fdt, which is clearly scaled with dt compared to $\sqrt{2D}dW = gdW$ which is scaled with $\sqrt{dt}$. This means that the equation-free analysis with large dt gives a more accurate approximation for f than for D: Since the fdt term dominates in magnitude the f approximation will be accurate, but the D approximation will be influenced by the fdt term. This implies that, for large δt, D will be particularly inaccurate where $|f|$ is largest, which in the case of the example SDE will be when $|x|$ is largest (see Figure 2.5 (B) overleaf). On the other hand when δt is smaller (implying dt is smaller) the term $\sqrt{2D}dW = gdW$ is dominant in the SDE since dW scales with $\sqrt{dt}$. So the noise term is dominant and this gives an approximation to D which is much more accurate than before as it is influenced by the drift term much less and an approximation to f which is less accurate since noise plays a much larger role in the approximation. A comparison of the approximations to f and D is given in Figure 2.5 overleaf.

Equation-free analysis gives a method of approximating the drift and diffusion terms for the previously unknown underlying SDE describing the identified switching behaviour. Once the drift and diffusion have been calculated they can be used to calculate the mean switching time and further moments of the switching time as illustrated in Section 2.7. The first step towards this is to calculate the approximated potential; recall that $\frac{f(x)}{D(x)} = -\phi'(x)$ and hence numerically integrate $\frac{f(x)}{D(x)}$ (see Figure 2.6 on page 25).

Since a good approximation to the potential is known the usual analysis could be used to find the SPD and the mean switching time. However, since there is such an obvious

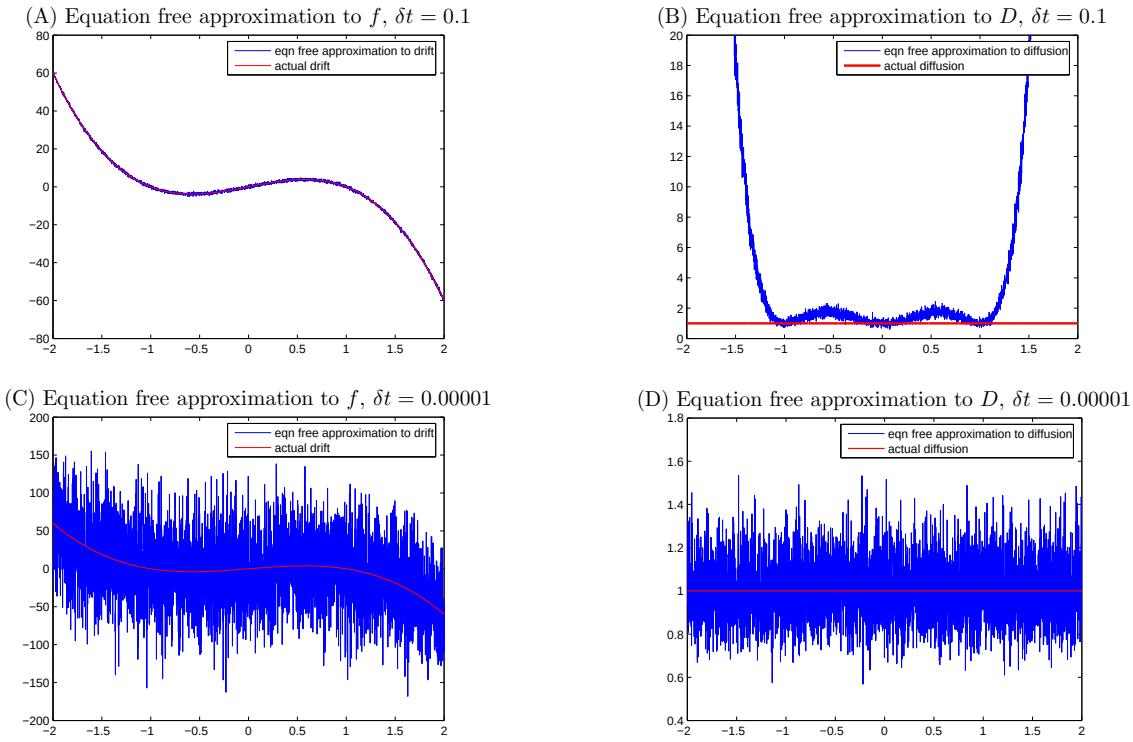


Figure 2.5: *Equation-free approximations to the drift and diffusion terms of SDE (2.9.1) plotted with the actual drift and diffusion terms. NOTE: Scales on the y-axis are not the same for plots (A), (B), (C) and (D). It is clear that for* $\delta t = 0.1$ *the drift term is approximated very well (so much so that the actual drift term plotted in red in (A) can hardly be seen), but that the diffusion approximation (B) is not very accurate at all, especially at the extremities where* $|x|$ *is largest. Conversely for* $\delta t = 0.00001$ *although both the drift and diffusion terms appear noisier, the diffusion term in (D) is approximated much more accurately than it was in (B) with larger* δt*. On the other hand the approximation to the drift term in (C) is far worse than in (A). It is clear that for different values of* δt *an accurate approximation to both* f *and* g *can be achieved. All of the above drifts and diffusions were found using the code* `myeqnfree.m`.

similarity between the equation-free derived potential and the actual potential (see Figure 2.6 overleaf) I can be satisfied that the equation-free method will provide a suitable potential for such calculations and hence I will omit them here.

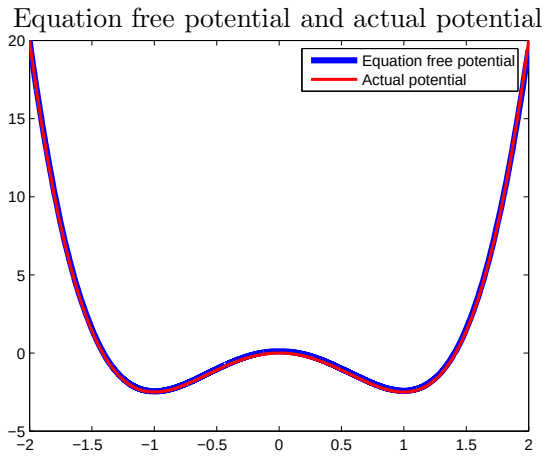


Figure 2.6: *Equation-free approximation to the potential plotted with the real potential. The red line represents the actual potential and the blue line represents the equation-free approximation to the potential with* $\delta t = 0.1$. *Such is the similarity between the two curves that I have had to plot the equation-free approximation to the potential with double line thickness so it can be seen. The constant of integration was chosen so that the actual potential and the equation-free potential would overlap for a good comparison. However the constant would usually not be known and as far as the SPD and switching moments are concerned is not important. The potential was found using the code* `myequationfreepotenital.m`.

Chapter 3

Self-Propelled Particle Models

Self-propelled particles (SPPs) (as they will be used in this project) are, as described in [26], particles whose velocities are determined by a simple rule and random fluctuations. The only rule of the model is *at each time step a given particle assumes the average velocity of the particles in its neighbourhood of radius r with some random perturbation (noise) added*[1] [26]. The term neighbourhood in the previous sentence can refer to one, two or even three dimensions with the neighbourhood being a line segment, a circle or a sphere respectively (although this project will deal only with one and two dimensions). Throughout the rest of the project the term 'neighbour' will refer only to those particles inside the interaction neighbourhood of the particle in question including or excluding the particle itself as will be made obvious by the context.

There are systems of self-propelled particles in which there are attraction terms and repulsion terms between the particles, and indeed (in two or three dimensions) in which the interaction neighbourhood is a more complicated shape i.e. a section of a circle or sphere [27]. However, this project will be limited to systems with simple interaction neighbourhoods and the very simple interaction rule given above.

3.1 Variation of Alignment with Interaction Radius

Before I begin discussion of the actual models themselves it is important to make clear the concepts of alignment and phase. Later I will need to consider the alignment of the particles. Alignment is simply a measure of the average direction of motion of all the particles. The particles will interact according to the simple rule, given above (in italics) and in [26], updating their positions and velocities at each time-step. When the particles have interacted for a sufficient number of timesteps the process is stopped; this whole process is known as one simulation. Let the time for the total simulation be T and the

[1] There is some debate as to where the noise term should be added in order best to model particles realistically. In both [7] and [26] (and in the 1-D model in this project) the noise term is added after averaging the local velocities that the particle measures, indicating that the particle's error comes in the implementation of the 'perfectly' measured velocities. However, it should be noted that in their paper, [15], Guillaume Gregóire and Hugues Chaté argue that for modelling reasons they changed the way that noise is incorporated into their system: As opposed to making an error when trying to take the direction they have 'perfectly' calculated ('angular noise') particles make errors when estimating the neighbouring velocities, for example, because of a noisy environment [15]. A recent paper by Aldana et al [1] indicates that the nature of the phase transition depends critically on the way in which noise is introduced into the system. Fortunately in this project I will not be concerned with the nature of the phase transition, merely the fact that one exists (see Section 3.1).

number of timesteps be J, meaning that the time between two timesteps t_{j-1} and t_j is $dt = T/J$. Each simulation will produce an alignment value by averaging the alignments at each time step over the second half of the time steps for the simulation: $t_j = \frac{T+2}{2}, \ldots, T$. The reason why alignments are averaged over the second half of the simulation is that the particles are initialised with random directions and if insufficient 'warm up time'[27] is allowed then the initial conditions may play too significant a role in the overall alignment. By discarding the alignments for the first half of the time steps the simulation is allowed to reach a consistent state or 'warm up'. In one dimension the alignment at each time step, $\zeta(t_j)$ will be given by the average velocity of the particles;

$$\zeta(t_j) = U(t_j) = \frac{1}{N}\sum_{i=1}^{N} u_i(t_j) \tag{3.1.1}$$

where $u_i(t_j)$ is the velocity of the ith particle at time t_j. For example $\zeta(t_j) = 0$ indicates no overall alignment and $\left|\zeta(t_j)\right|$ close to 1 indicates large alignment of all the particles in either direction. The alignment for one simulation will be given by

$$\zeta_{overall} = \frac{\sum_{j=J/2+1}^{J} |\zeta(t_j)|}{J/2}, \tag{3.1.2}$$

In two dimensions the alignment at each time step will be given by

$$\zeta(t_j) = \frac{1}{Nu}\left|\sum_{i=1}^{N} \mathbf{u}_i(t_j)\right|, \tag{3.1.3}$$

where u is the constant speed of all the particles. The overall alignment for the whole simulation in two dimensions will also be given by equation (3.1.2).

The concept of overall alignment is essential when considering phase. The crucial metaphor here is SPPs being particles of matter, and is easier to visualise in two dimensions. For example if the SPPs move around randomly with no ordered motion whatsoever then they are said to be in the *gas* state. If the particles move around in small groups often breaking off from the group to form other groups then the particles are said to be *liquid*. If the particles all move in the same direction varying their position with respect to the other particles only slightly, so that in a frame moving at the average velocity of the particles it looks as if the particles are not moving except for some small vibrations, then the particles are said to be in the *solid* state. The concept of phase transition for SPPs is exactly analogous to phase transition for particles of matter. There are the two obvious phase transitions, 'gas-liquid' and 'liquid-solid' and of course their reverse processes, but there is also the idea of vaporisation; the 'solid-gas' transition and its reverse. In order to measure the phase of the particle system alignment, $\zeta_{overall}$, will be used.

In order for there to be a phase transition a parameter must be varied. In [7], both density and noise terms are varied to give phase transitions. With specific fixed parameter values (noise, η, and density, ρ) a phase transition can be achieved by varying the interaction radius (IR), r. Figure 3.1 below clearly shows an example of such a phase transition for the one dimensional model. The system goes from being disordered to highly ordered over a small range of interaction radii (IR)[2], so the phase transition is said to be sharp.

[2]IR will be used throughout the project as an abbreviation for both interaction radius and interaction radii. The context will make it clear which one is intended.

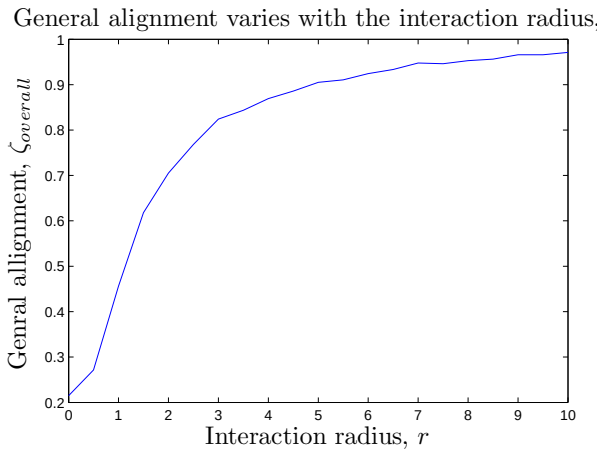


Figure 3.1: *Variation of the alignment, $\zeta_{overall}$, for a one dimensional SPP model with the IR of the particles. A phase transition can clearly be seen between $r = 0$ and $r = 3$. The particles go from being a generally unaligned 'gas' at r=0 through the 'liquid' state between $r = 0.5$ and $r = 2.5$ and into the highly aligned 'solid' state for $r \geq 3$. This phase change was found using the code* `czirokfixedalpharepeat.m` *. In two dimensions (from whence phase change analogy originates) it is easy to see the difference between the phases of the particles. I have included four movies on the CD accompanying this project to help illustrate the differences in phase for a two dimensional group with and without a leader (see Chapter 5). They are intended as an aid to visualisation but it is not necessary to view them to understand the concepts of phase.*

Now that the concepts of phase transition and alignment are clear I will go on to discuss the models in more detail.

3.2 One-Dimensional Model

The one dimensional model I will use will be based around the model given in Czirók et al [7]. Consider N off-lattice particles along a line of length L with periodic boundary conditions. Particle i for $i = 1, \ldots, N$ is distinguished by its lateral coordinate x_i and by its velocity u_i. The time unit $\Delta t = 1$ was chosen to be the time between two updatings of position and velocity. These two properties of each particle are updated according to the rules: [7]

$$x_i(t + \Delta t) = x_i(t) + \Delta t u_i(t), \tag{3.2.1}$$

$$u_i(t + \Delta t) = u_i(t) + \Delta t[G(\langle u(t)\rangle_i) - u_i(t)] + \Delta Q. \tag{3.2.2}$$

Here

$$\langle u(t)\rangle_i = \frac{1}{|\mathcal{J}_i^r|} \sum_{j \in \mathcal{J}_i^r} u_j(t) \tag{3.2.3}$$

is the local average velocity for the ith particle and $\mathcal{J}_i^r \equiv \mathcal{J}_i^r(t)$ is the set of all $j \in 1, 2, \ldots, N$ such that $|x_i(t) - x_j(t)| \leq r$, where r is the IR [10]. The function G represents the adjustment of a particle's velocity to the velocity of its neighbours [4]. In the paper by Czirók et al [7] the function G is not defined when the argument is zero so instead I will take G to be defined as in [10];

$$G(z) = \frac{1}{1+\beta}\begin{cases} z+\beta, & \text{for } z > 0; \\ 0, & \text{for } z = 0; \\ z-\beta, & \text{for } z < 0, \end{cases}$$

where $\beta \in (0, \infty)$ is a parameter that needs to be specified. As in [4] and [7] I chose the simplest case $\beta = 1$ (see Figure 3.2). The noise term ΔQ, is a random number (different for

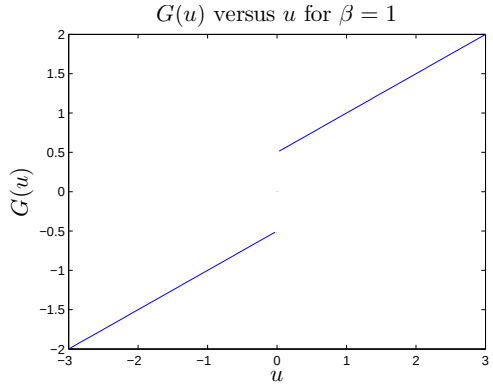


Figure 3.2: *A plot of $G(u)$ versus u for $-3 \leq u \leq 3$ and with $\beta = 1$.*

each i) from the uniform distribution:

$$Q(x) = \begin{cases} 0, & \text{for } x < -\frac{\xi}{2}; \\ \frac{1}{\xi}, & \text{for } \frac{-\xi}{2} \leq x \leq \frac{\xi}{2}; \\ 0, & \text{for } x > \frac{\xi}{2}, \end{cases}$$

with mean 0 and variance $\frac{\xi^2}{12}$. The size of the noise $\xi(\Delta t)$ can be varied in order to change the nature or position of the phase transition. The size of the density term will also make a substantial difference to the results obtained. In my work I will keep both the size of the noise and density fixed to a value which will give a phase change over values of r which are of order one. In the one dimensional case the density will be chosen as the approximate density at which switching occurred in Buhl et al's locust experiment [4]: $\rho = \frac{1}{3}$ particles per unit length. This density is also typical of locusts in the field. I have found through experimentation with Matlab code that this density implies that I should take $\xi(\Delta t) = 3(\Delta t)^{\frac{1}{2}}$ (= 3 since I will choose $\Delta t = 1$) in order to achieve a phase transition for IR, r, of order one (see Figure 3.1 above). It is also important to note that for a consistent model as $\Delta t \to 0$ it is required that $\xi \sim (\Delta t)^{\frac{1}{2}} \to 0$, (see footnote 2 Chapter 2).

As well as varying r I initially considered whether the weighting the particle gives to its own velocity compared to that of the averaged measured velocity of its neighbours had an effect on the alignment of the particles [10]. Adding this weighting factor to the model, the new velocity update equation is given by

$$u_i(t+\Delta t) = u_i(t) + \Delta t\left[G\left(\frac{\alpha}{n(t)+\alpha}u_i(t) + \frac{1}{n(t)+\alpha}\Big[\sum_{j\in\mathcal{J}_i^r} u_j(t) - u_i(t)\Big]\right) - u_i(t)\right] + \Delta Q, \quad (3.2.4)$$

where $n(t) = |\mathcal{J}_i^r(t)| - 1$ is the number of neighbours of the ith particle, excluding itself. (Choosing $\alpha = 1$ gives the original velocity update equation.) However, when I plotted

the alignments for varying values of α and r I found that even varying α between 0 and 5 had very little effect on the overall alignment of the particles (see Figure 3.3) so it was considered best to keep the weighting fixed at $\alpha = 1$ (i.e. all the particles are given equal weighting) and simply to vary r.

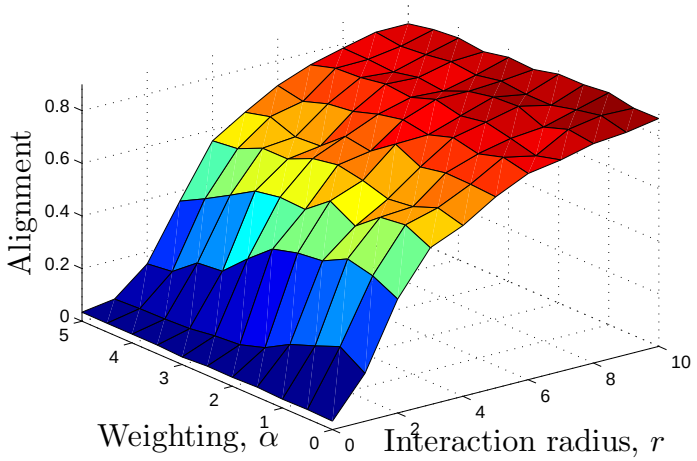


Figure 3.3: *A surface plot of alignment varying with IR, r and weighting parameter, α. There are small variations in the alignment as α is varied, but they are not significant enough to justify varying the weighting parameter. The alignment varies significantly with IR, r, from 0 when r is zero (as expected), to nearly 0.9 when r reaches 10. The code used to find these results was* `czirokspacerepeat.m`.

3.3 Application of the Equation-Free Method to the One Dimensional Model

In the one dimensional model I am trying to replicate qualitatively the behaviour found in [4]. The alignment term at each time step, $\zeta(t_j)$ will be similar to the instantaneous alignment Φ^t of [4] calculated for each camera image.

I wrote the Matlab code `czirok.m` (named after the first author of the paper in which the model was first described) to implement the model described at the start of this chapter, for self-propelled particles moving in one dimension [7]. The Figures 3.4 (A) and (B) show an implementation of this code with IR $r = 4$, noise $\xi = 3$ and 30 particles on a domain of length 90 giving density $\rho = \frac{1}{3}$. Figure 3.4 (A) shows the paths of each of the 30 particles against time and Figure 3.4 (B) shows the general alignment of all thirty particles against time.

Figure 3.4 (B) shows obvious qualitative similarity to the experimental switching behaviour depicted in Figure 1.1 (B) and the switching behaviour of model SDE, in Figure 2.3 (B). The main qualitative difference between Figure 3.4 (B) and Figure 1.1 (B) is that the alignment in Figure 3.4 (B) can take values greater than one. This is due to the fact that, in the code `czirok.m` , un-normalised alignments ζ and $\zeta_{overall}$ are considered (see (3.3.1) and (3.3.2) respectively), whereas in the experiment that gives rise to Figure 1.1 (B) the alignment can clearly not be greater than one, as an alignment greater than one has no

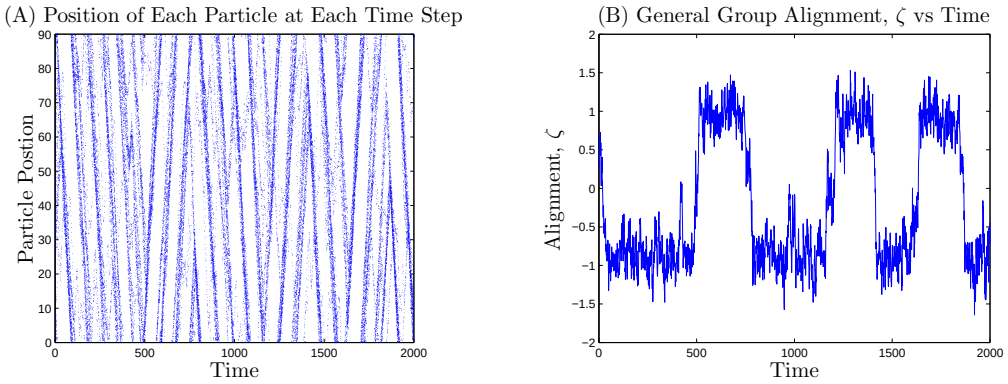


Figure 3.4: *(A)The position of each particle at each time step. (B) Un-normalised alignment, ζ varies with time. The effect of (A) is to show the general direction of motion for the group. It is easy to see that most of the time almost all of the particles are travelling in the same direction as each other, although this direction changes (switches) over time. There is a qualitative similarity between (B) and Figure 1.1 (B), in so far as switching is exhibited. The main difference is that the average switching time appears to be longer. This is simply a matter of scaling. The code for the 1-D SPP model which produced these two figures is* `czirok.m`.

physical meaning[3].

As one of the aims of this project I wanted to have a model that is predictive as well as descriptive. In the Czirók model I have exactly that. I will use the model to make a prediction about the experimental results and then compare with the actual experimental data. Due to the nature of the experimental result this prediction will be qualitative rather than quantitative, but it will be a good test of the behaviour of the Czirók model. If Figure 1.1 (B) the density of the locusts is $\frac{1}{3}$ locusts per unit length and the alignment switches four times in a total time of around 450 giving an approximate switching time of 112.5 time units. In the model I also use the density $\frac{1}{3}$ particle per unit length to achieve 7 switches in a time of 2000 giving a switching time of 285.7 time units[4]. I want to use the model to predict what will happen when I increase the density of particles to 1 particle per unit length. Re-running the model with $\rho = 1$ I found that the are no switches in a time period of 2000 timesteps (see Figure 3.5 (B) below) which equates to 800 timesteps in the experimental model. Compare this prediction of no switches in the model to the experimental results for density $\rho = 1$, which translates as no switches in a time period of 800. Although the experimental data does not extend over such a long time period, it would certainly be expected that there are no switches in the shorter time length that the experiment runs for. The experimental data for density $\rho = 1$ agrees with the prediction, showing that no switching is exhibited (see Figure 3.5 (A) below). This shows that, although in this case the prediction was only qualitative, the model is capable of making valid predictions, and hence is far more useful than a purely descriptive model.

The similarity of the alignment profile for the Czirók model, in Figure 3.4 (B), and numerical simulation of the example SDE in, Figure 2.3 (B), gives rise to the hypothesis that there is an underlying SDE for generating the alignment of the particles in the Czirók

[3]To make the `czirok.m` code a more realistic model of the locust behaviour the alignment could be normalised, but the equation-free results presented next will generate potentials which are easier to compare qualitatively if the alignment is left un-normalised.

[4]As I noted before, this switching time could be made the same by a simple rescaling of the model. In this case simply make the time units of the model around 2.5 times longer to make the switching times approximately the same.

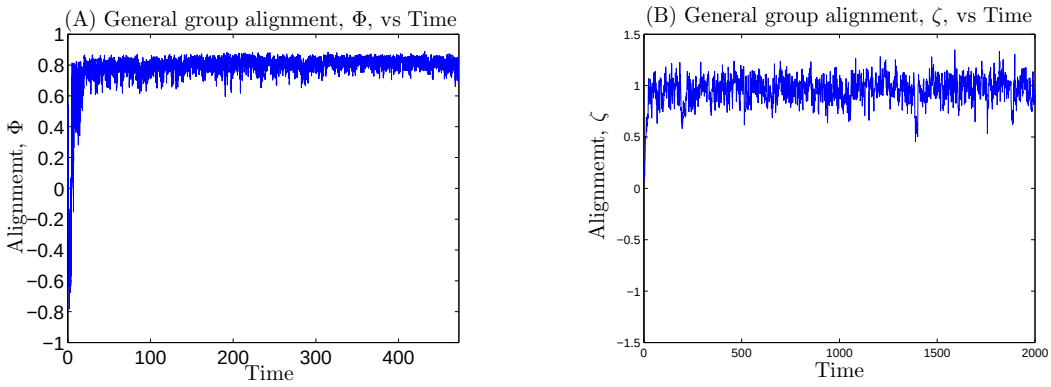


Figure 3.5: *(A) Experimental and (B) modelled results for locust density $\rho = 1$. A clear qualitative similarity is exhibited between the experimental results and the simulation. Most importantly no switching is observed in either.*

model, with, as yet, unknown drift and diffusion terms. Equation-free analysis can be used to determine these properties, which in turn will enable the underlying potential to be found. I will compare the potential derived using the short-time equation-free analysis with the long-time equation-free analysis (see Section 3.5) to check for consistency.

Using the short-time equation-free techniques as described in Section 2.9 I wrote the code `czirokeqnfreepotential.m` in Matlab to find the drift and diffusion terms and hence from those to find the underlying potential for the alignment of the particles (using equation (2.6.7)). I also wrote `czirokeqnfreepotentialstatprob.m` and `czirokstatprobbars.m` to compare the SPD of the alignment predicted by the equation-free technique and SPD computed by taking a sample of alignments when the simulation was allowed to run for a long time and plotting their frequencies in a histogram as in Figure 2.4 (page 16). The results of the codes are given in Figures 3.6 and 3.7:

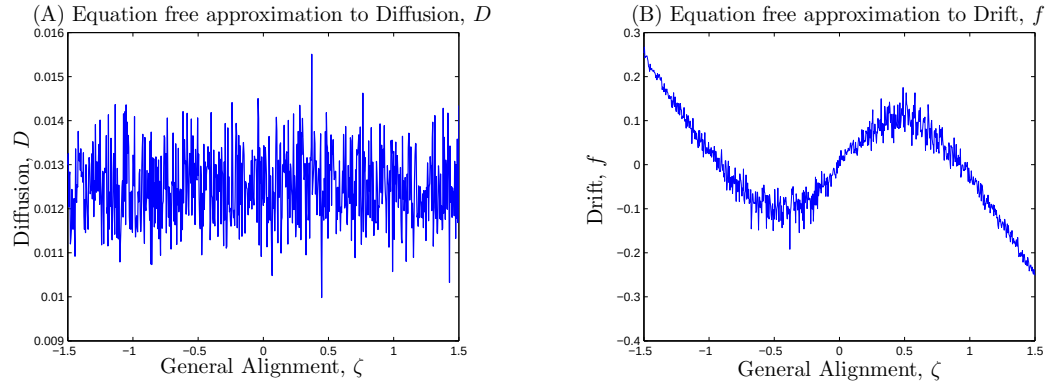


Figure 3.6: *The diffusion and drift and potential for the Czirók model found using equation-free techniques.*

The fact that the potential derived using the equation-free technique is double welled (see Figure 3.7 (A) below) means that qualitatively, at least, I have found a potential for which the corresponding SDE will demonstrate switching behaviour. Further more the comparison of the SPDs generated using the equation-free method and the histogram method (see Figure 3.7 (B) below) confirms that quantitatively the potential derived must be very close to the actual potential since the derived SPD closely matched the SPD found by sampling the simulation.

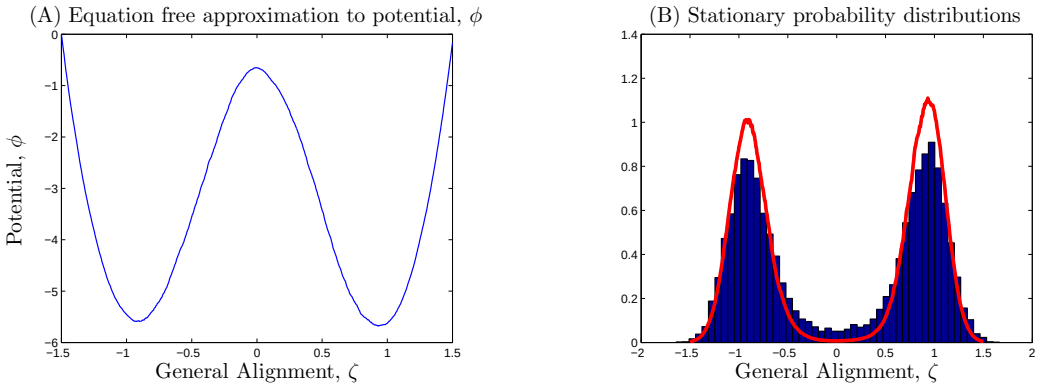


Figure 3.7: *(A)The potential for the Czirók model found using the equation-free technique. (B) SPD for the Czirók model found using the equation-free technique compared to the SPD found using the histogram method (originally described for Figure 2.4).*

Computing the mean switching time for the Czirók model using the potential from the equation-free method and the exact equation (2.8.3) from Section 2.8 a value of 153.98 (2 d.p.) is found. Compare this to the switching time found by running the code `czirokswitchtime.m`, which finds the first time the alignment, ζ, becomes greater than zero, given that it starts at $\zeta = -1$ (the bottom of the potential well) and averages over 10,000 repeats. Using this method, a value of 154.21 (2 d.p.) is found.

Method	Equation-free Method	Repeated Sampling
Mean Switching Time	153.98	154.21

Table 3.1: *A comparison of two methods of finding the mean switching time for the Czirók model with noise $\eta = 3$, density $\rho = \frac{1}{3}$ particles per unit length and IR, $r = 4$. The first time was found using equation-free methods to find the potential of an assumed underlying SDE and then an exact formula derived from the backwards Kolmogorov equation to find the switching time. The code I used was* `czirokeqnfreepotentialswitchingtimes.m` *. The second method runs the Czirók code with initial average alignment $\zeta = -1$ until the alignment reaches $\zeta = 0$. At this point the time is recorded and the process starts again. This process was repeated* $10,000$ *times and a mean switching time calculated as an average of all these times. For this I used the code* `czirokswitchtime.m` *.*

These values are remarkably close providing yet further evidence that the potential derived using the equation-free methods is accurate.

3.4 Application of the Equation-Free Method to the Full Interaction SPP Model

It would be useful to have a further vindication of the method using an analytical result that does not depend on a computer code, which can be directly compared with results from the equation-free analysis. Fortunately there is a specific case of the Czirók model in which all particles interact with each other at every step, (i.e. the IR is large enough to cover the whole domain[5]) which can be analysed in order to find an exact equation for the

[5]This is not a realistic situation in nature (as, for example, in locust marching bands hundreds of thousands of locusts cover a large area) but it will be a useful validation of the model.

potential and hence the SPD and switching time. This can then be compared with results from the equation-free analysis of the code with such a large IR and used to validate the previous results.

Recall that the velocity update equation for each particle in the model is given by (3.2.4):

$$u_i(t+\Delta t) = u_i(t) + \Delta t\left[G\left(\frac{\alpha}{n(t)+\alpha}u_i(t) + \frac{1}{n(t)+\alpha}\Big[\sum_{j\in\mathcal{J}_i^r} u_j(t) - u_i(t)\Big]\right) - u_i(t)\right] + \Delta Q,$$

where $n(t) = |\mathcal{J}_i^r(t)| - 1$ is the number of neighbours of the ith particle, excluding itself and, as before, ΔQ is a random number chosen from the uniform distribution, $Q(x)$ given in Section 3.2. It was demonstrated earlier that varying α between 0 and 5 made little difference to the values of the phase change as r varied, so essentially any $0 \le \alpha \le 5$ can be chosen without loss of generality. This is a result which has not been presented in the literature for one dimensional self-propelled particle models before. Here, for convenience of working I choose $\alpha = 0$. Since it is now assumed that the IR, r, covers the whole domain, this implies that the particle gives weight to the previous velocities of all the particles in the simulation. In this case $n(t) = N - 1$ for all t, where N is the total number of particles in the simulation. Substituting this and $\alpha = 0$ into (3.2.4) gives the new velocity update equation,

$$u_i(t+\Delta t) = u_i(t) + \Delta t\left\{G\left[\frac{1}{N-1}\sum_{j\neq i} u_j(t)\right] - u_i(t)\right\} + \Delta Q, \quad i = 1, 2, \ldots, N. \tag{3.4.1}$$

Equations (3.4.1) are not coupled with the position update equation (3.2.1) because it was assumed the number of particles in the simulation is fixed and equal to N. Consequently, the system of particles (in a frame co-travelling with the band of aligned particles) can be described by the system of N stochastic differential equations (3.4.1) [9]. Define the alignment at time, t, as before (3.3.1),

$$\zeta(t) = U(t) = \frac{1}{N}\sum_{i=1}^{N} u_i(t_j), \tag{3.4.2}$$

where $U(t)$ is the average velocity.

Since G is a piecewise linear function (see Figure 3.2 page 29), write

$$G\left[\frac{1}{N-1}\sum_{j\neq i} u_j(t)\right] = G\left[\frac{N}{N-1}U(t) - \frac{u_i(t)}{N-1}\right] =$$

$$= G\left[\frac{N}{N-1}U(t)\right] - \frac{u_i(t)}{(N-1)(1+\beta)} + \frac{1}{1+\beta}\begin{cases} -2\beta, & \text{for } u_i(t) > (N-1)U(t) > 0; \\ +2\beta, & \text{for } u_i(t) < (N-1)U(t) < 0; \\ -\beta, & \text{for } u_i(t) = (N-1)U(t) > 0; \\ -\beta, & \text{for } u_i(t) > (N-1)U(t) = 0; \\ +\beta, & \text{for } u_i(t) = (N-1)U(t) < 0; \\ +\beta, & \text{for } u_i(t) < (N-1)U(t) = 0; \\ 0, & \text{otherwise.} \end{cases} \tag{3.4.3}$$

The last term in (3.4.3) can only be non-zero if $|u_i(t)| \ge (N-1)|U(t)|$. Assume that this is never the case and will neglect this final term in what follows [9]. Rewrite equations (3.4.1)

as

$$u_i(t+\Delta t) = u_i(t) + \Delta t\left\{G\left[\frac{N}{N-1}U(t)\right] - u_i(t)\left(1+\frac{1}{(N-1)(1+\beta)}\right)\right\} + \Delta Q, \tag{3.4.4}$$

where $i = 1, 2, \ldots, N$. Adding equations (3.4.4) and dividing through by N gives

$$U(t+\Delta t) = U(t) + \Delta t\left\{G\left[\frac{N}{N-1}U(t)\right] - U(t)\left(1+\frac{1}{(N-1)(1+\beta)}\right)\right\} + \frac{\xi}{\sqrt{12N}}\Delta W, \tag{3.4.5}$$

where ΔW is now a random number chosen from the normal distribution $N(0,1)$. The last term in equation (3.4.5) comes from using the central limit theorem for a sum of distributions assuming that N is sufficiently large to justify its use[6]:

$$\sum_{i=1}^{N} Q_i(x) = \left(\sum_{i=1}^{N} \mathrm{var}(Q_i(x))\right)^{1/2} N(0,1) = \sqrt{\frac{N}{12}}\xi N(0,1),$$

where the $Q_i(x)$s are identical uniform distributions, with mean 0 and variance $\frac{\xi^2}{12}$ as in Section 3.2. Equation (3.4.5) is a discretised version of the SDE

$$dU = \left\{G\left[\frac{N}{N-1}U(t)\right] - U(t)\left(1+\frac{1}{(N-1)(1+\beta)}\right)\right\} + \frac{\xi}{\sqrt{12N}}dW. \tag{3.4.6}$$

Let $P(U,t)$ be the probability distribution function of random variable U. Given the appropriate initial condition $P(U,0)$, it can be computed as a solution of the F-P equation, (see Section 2.5 equation (2.5.18)),

$$\frac{\partial P}{\partial t} = \frac{\partial}{\partial U}\left(\frac{\xi^2}{24N}\frac{\partial P}{\partial U} - P\left\{G\left[\frac{N}{N-1}U\right] - U\left[1+\frac{1}{(N-1)(1+\beta)}\right]\right\}\right). \tag{3.4.7}$$

As before (see Section 2.6 equation (2.6.4)) the steady solution to (3.4.7) is given by

$$P_s(U) = C\exp\left[-\phi(U)\right], \tag{3.4.8}$$

where $C^{-1} = \int_{-\infty}^{\infty}\exp\left[-\phi(U)\right]dU$ and the potential $\phi(U)$ can be computed as

$$\begin{aligned}
\phi(U) &= -\frac{24N}{\xi^2}\int_0^U G\left[\frac{N}{N-1}u\right] - u\left(1+\frac{1}{(N-1)(1+\beta)}\right)du = \\
&= -\frac{24N}{\xi^2}\left\{\frac{NU^2}{2(N-1)(1+\beta)} + \frac{\beta|U|}{1+\beta} - \frac{U^2}{2}\left(1+\frac{1}{(N-1)(1+\beta)}\right)\right\} = \\
&= -\frac{24N}{\xi^2}\left\{\frac{U^2}{2(1+\beta)} - \frac{U^2}{2} + \frac{\beta|U|}{1+\beta}\right\} = \\
&= \frac{12N\beta}{\xi^2(1+\beta)}\left(U^2 - 2|U|\right).
\end{aligned} \tag{3.4.9}$$

Clearly the potential $\phi(U)$ is symmetric with respect to $U = 0$ and has two global minima at $U_\pm = \pm 1$ [9]. Using the code `czirokequationfreepotential.m` and `czirokeqnfreepotentialstatprob.m` as before with the IR of each particle set to $L/2$, where L is the length of the domain, I approximated the potential and SPD of the underlying SDE using the equation-free methods discussed previously. The similarity between the analytically derived potential and SPD curves and the corresponding equation-free derived curves is clear (see Figure 3.8 page 36).

[6] In my one dimensional code N=30 which is large enough to justify the use of the central limit theorem.

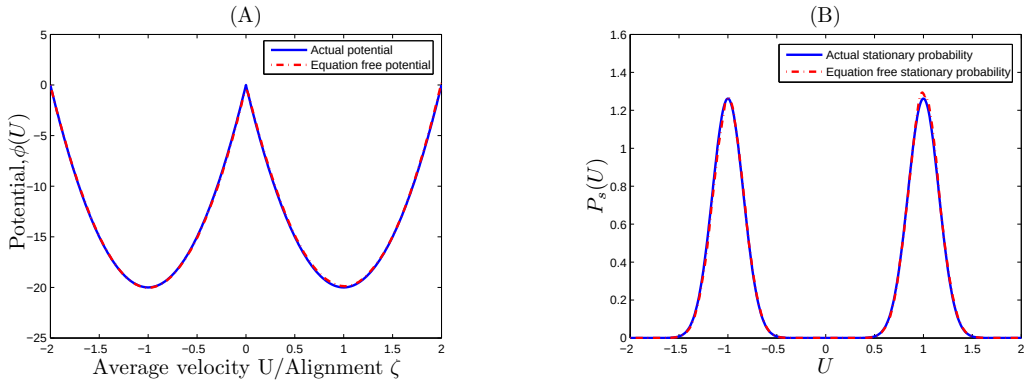


Figure 3.8: *The potential and SPD for a special case of the Czirók model (the IR covers the whole domain). The blue lines in figures (A) and (B) are the analytically derived potential and SPD respectively. Such is the accuracy of the approximation that the red lines, representing the equation-free approximations to potential and SPD respectively, has to be dotted in order to be able still to see the blue lines.*

3.5 Long-Time Equation-Free Analysis

In reality (Buhl et al's locust experiment for example) the equation-free technique (described in Section 2.9 and applied above) of initialising the particles at a large number of different possible alignments (so as to get smooth curves for the drift diffusion and potential) and running the experiment repeatedly for a very short time is not practical. However, there is another way to approach the problem. Simply run the experiment for a long time and record the alignments at each step. Then, provided there are a sufficient number of switches, timesteps which exhibit the whole range of alignments can be chosen and these can simply be taken to be the initialisations [16]. Then consider the alignments a short time δt later and carry out the same analysis as before. The down side to this method is that all possible alignments must be exhibited in the experiment and if no switching is exhibited (see Figure 1.1 (C) page 2) then this technique will not work. The drift, diffusion (and hence potential) can only be found for alignments in the range which the experiment takes as opposed to in the one dimensional SPP model where it was possible to find the potential for a much wider range of alignments, however unnatural they may be. Also a significant number of switches are required for the long-time method. This is because, although it will be easy to estimate the drift and diffusion near the potential *wells* as the alignment will spend a long time there, the alignment will only be near the potential *barrier* when the alignment switches from positive to negative. In order to get a good approximation for drift and diffusion, for alignments near the potential barrier (using formulae (2.9.2) and (2.9.4)) the process will need to switch a sufficient number of times. This means that the simulation or experiment will have to run for a long time, which was not true of the previous equation-free method. The problem of not having enough data points may also be encountered at the extremities of the alignment, leading to the necessity of artificially reducing still further the range of alignments for which the potential can be found. This method does, however, have a two fold benefit. Firstly using long-time stochastic simulation means that there is no need to carry out the complicated process of initialisation which would be especially difficult in experiments with real animals. Secondly, the initialisation alignments used will be inherently natural: there is always a tendency, when initialising the SPPs to give them some form of predetermined unrealistic velocities in order to get the required alignment

needed for the equation-free analysis[7]. Taking initialisation velocities from the long-time simulation, however, will inherently give a realistic spread of alignments for the particles.

The drift, diffusion and potential for the Czirók model with the same parameter values as were used for the short-time equation-free methods are given in Figures 3.9 and 3.10 below. I also calculated the SPD and compared it with the alignment histogram found in the same way as Figures 2.4 and 3.7 (B). To create these figures I used the codes `cziroklongeqnfreeefficientsplit.m`, `myswitchprobeqnfree.m` and `stationaryprobabilityeqnfree.m`.

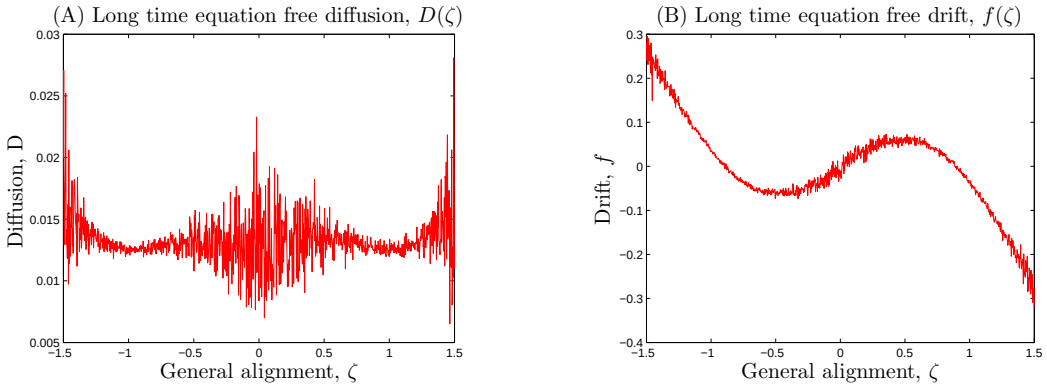


Figure 3.9: *The diffusion and drift terms of the SDE supposedly underlying alignment of the particles in the model, calculated using the long-time equation-free technique.*

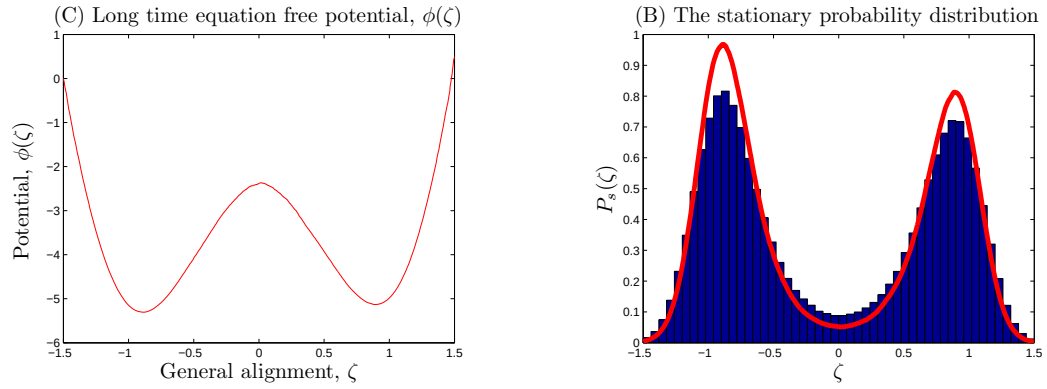


Figure 3.10: *The potential and SPD derived using the long-time equation-free technique. In (B) the derived SPD is also compared with the probability distribution histogram, derived by sampling the alignment of the long-time simulation at evenly spaced time intervals and plotting these values in a histogram.*

It is clear to see that the equation-free potential is double welled as expected and that the SPD derived using the long-time equation-free technique is a good representation of the actual SPD. Both of these factors inspire confidence in the long-time equation-free technique.

[7]For example in the code `czirokeqnfree.m` the initialisation used was initially to give all the N particles the same velocity (which was the same value as the required alignment), then to add some $N/2$ random numbers (one each) onto the velocities of the first $N/2$ particles and take the same random number away from the velocities for second $N/2$ particles, thus leaving the mean velocity for all particles unchanged. Although this is better than just leaving all the particles with the same initial velocity it is still not particularly realistic.

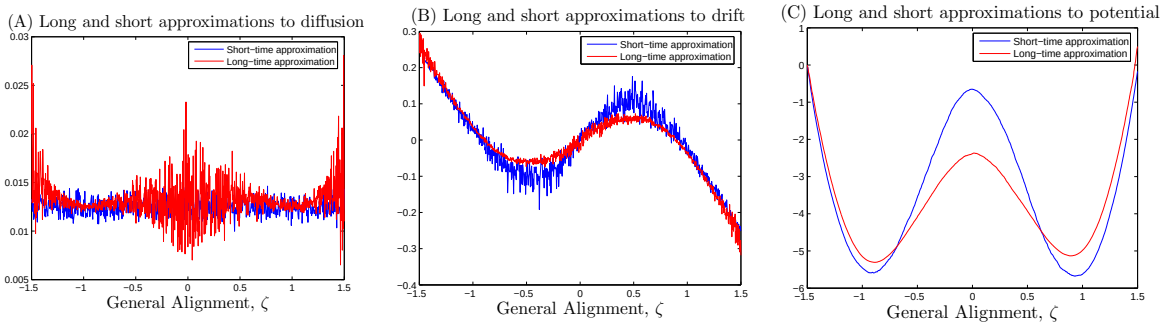


Figure 3.11: *A comparison of the diffusion, drift and potential of an assumed underlying SDE for alignment of the particles in the Czirók model derived using the two equation-free methods. The blue lines give the short-time equation-free approximation and the red lines the long-time equation-free approximation.*

Figure 3.11 shows that the two methods clearly give very similar results. A possible reason for the disparity between the two potentials at the potential barrier, in Figure 3.11 (C), is that, as mentioned earlier, there are far fewer points with alignments in that area to be sampled[8], so the equation-free drift and diffusion and hence the potential (which depend on mean values) will be less accurate. It is clear to see that in Figure 3.11 (A) the diffusion becomes very noisy around this area. Despite these small discrepancies the two potentials compare well giving confidence in both the equation-free methods.

The above results (Figures 3.6 to 3.11 pages 32-38) together with the similarity of the switching times (Table 3.1) are a two fold vindication of the project thus far. The fact that the equation-free methods reproduce accurately the potential and the SPD of the 1-D SPP model with large IR (see Figure 3.8) means that the equation-free methods are both accurate and reliable. They are also exceptionally powerful tools, producing the drift and diffusion terms for an underlying SDE in a one dimensional model which simply exhibits switching behaviour and hence quantifying the model's behaviour allowing analysis, such as finding the mean switching time, to be carried out. The similarity of the calculated switching times (see Table 3.1) goes even further towards validating the equation-free technique. Further evidence of the reliability of the equation-free technique is given in [10]. The fact that reliance can be placed on this technique, means that the potential displayed in Figure 3.6 (B) is an accurate representation of the underlying potential of the Czirók model. The fact that this potential is double welled implies that the Czirók SPP model has inherent switching behaviour similar to the locust experiment in [4] and in turn implies that SPP models are realistic for modelling flocking behaviour[9]. The realistic nature of self-propelled particles will be important for the rest of the project.

Demonstrations of the reliability of the equation-free technique when there are other sources of corroboration of the results have shown it to be a reliable technique. I will now apply the long-time equation-free technique[10] to the experimental data found in [4] to

[8] Out of 1,000,000 sample points 2135 with alignment $\zeta = -1 \pm 3/2000$ (near the bottom of the potential well) compare to only 250 had alignment $\zeta = 0 \pm 3/2000$ (at the top of the potential barrier). Even fewer still (23) were located at the extremities of the alignments; $\zeta = -1.5 \pm 3/2000$ and $\zeta = 1.5 \pm 3/2000$.)

[9] This is true at least in one dimension.

[10] As discussed before, the long-time equation-free technique is the only one that can realistically be applied to the locust experiment as the short-time technique would require complicated and time consuming initialisation.

extract the underlying potential and SPD associated with the switching behaviour of the alignment of the locusts, where there are no other sources of confirmation of the results. To do this I wrote the Matlab code `datalongeqnfree25.m`. I chose a locust density that has not been used so far in this project. The switching behaviour with 25 locusts is demonstrated in Figure 3.12 (experimental data kindly provided by J. Buhl).

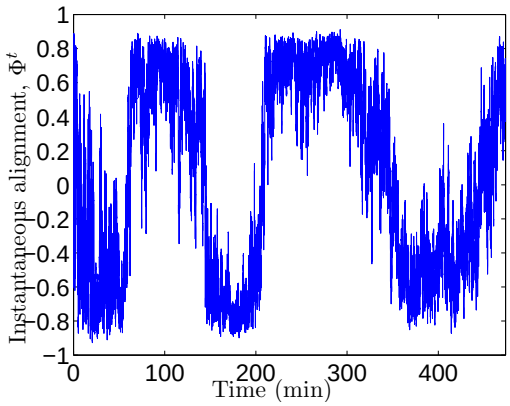


Figure 3.12: *Switching behaviour demonstrated in the sand ring experiment by Buhl et al with 25 locusts. This figure was plotted using the Matlab code* `locusts25.m`.

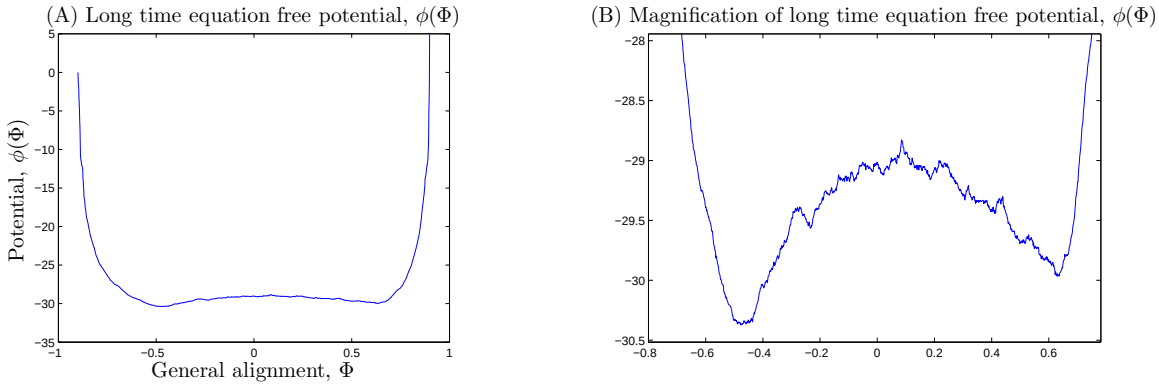


Figure 3.13: *(A) The potential for an experiment using the same techniques as in [4] but with 25 locusts. (B) A different scaling and cropping of figure (A). The potential derived from the experimental results looks different to the ones derived using the Czirók model. The main reason for this is the restriction on the values of the alignment. Theoretically in the Czirók model alignment can take any value, whereas in the experiment the absolute value of the alignment cannot possibly take a value greater than one. It is expected that the value of the potential to asymptotes to infinity at* $\Phi = \pm 1$ *as can be seen in(A). Despite the appearance of (A), a different scaling and crop, given in (B) show that a double welled potential still underlies the switching behaviour. The potential was found using* `locustslongeqnfree25.m`.

A potential for the experimental data has been found and exhibits the expected properties. The actual potential may look slightly different especially around the middling alignment values. This is an artefact of the experimental alignment switching relatively few times meaning there will not be enough samples around the middling alignment values to take an accurate mean.

Both SPDs for the experimental data (see Figure 3.14 (A)) are approximations to the actual underlying distribution and are both inaccurate in different ways. The long-time

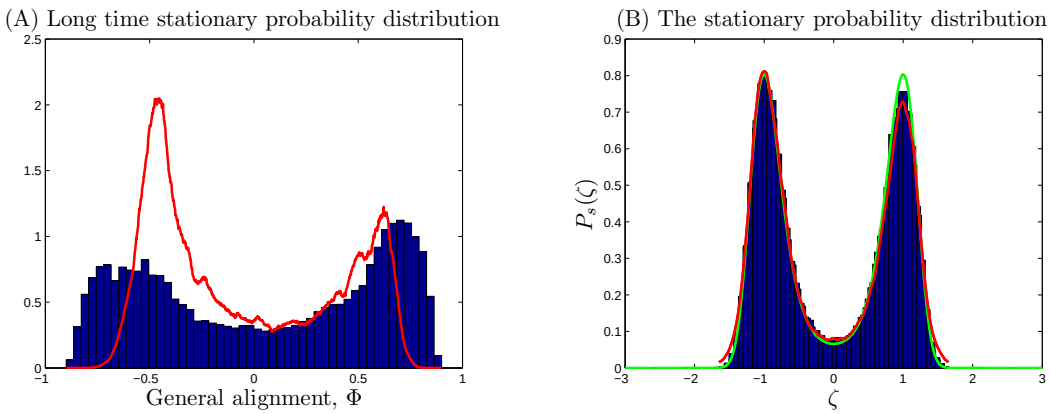


Figure 3.14: *Figure (A) shows two approximations to the SPD for the experiment with 25 locusts: the long-time equation free method in red and the simulation sampling to create a histogram. The SPDs were found using* `locustslongeqnfree25.m`. *Figure (B) shows three different methods of finding the SPD of the example SDE for a short-time simulation: the exact formula using the known potential (green), simulation sampling to create a histogram (blue) and the long-time equation-free method (red). These SPDs were found using the Matlab codes* `myswitchlongeqnfree.m` *and* `myswitchprob.m`.

equation-free SPD has peaks at alignment values -0.4 and 0.6, rather than -0.8 and 0.8 as may have been expected. The reason for this is that the alignment spends a large proportion of time (between t=350 and t=450 (see Figure 3.12)) around the alignment values of -0.4 and at various periods spends time near 0.6. Since the amount of data we have is relatively small, these sections of the simulation have a disproportionate effect on the long-time equation-free analysis. Although the SPD generated by the histogram method (as in Figure 2.4) has peaks in approximately the expected areas, it too suffers the effects of insufficient data. We would expect the stationary distribution to be symmetric about the potential barrier (at $\Phi = 0$,) but this is clearly not the case here.

For comparison I have also plotted the exact SPD for the example SDE from Chapter 2 using three methods (see Figure 3.14 (B)). The first is the exact formula (2.6.10) plotted in green, the second is the histogram approach, sampling the data from the simulation and the third, plotted in red is the long-time equation-free simulation method. The second two methods used data from a relatively short simulation of the SDE, which exhibited the same number of switches as in the experiment, to ensure a fair comparison.

It can be seen that the three methods give very similar results, so even for a short simulation the long-time equation-free method can be accurate. This may hint that the reason the SPD for the experimental data found by using the long-time equation free method does not match with the SPD found using the histogram method is that the assumption of an underlying SDE describing this data is not reliable.

Despite this worry, the experimental potential (see Figure 3.13) is interesting as the depths of the wells reflect how locked in to a particular direction the locusts are. The relatively flat potential for the experiment with 25 locusts reflects the relatively fast direction switches exhibited. A density of around 25 locusts reflects the density of locusts in the field. It may be that locust density has evolved so as to maximise the speed information transfer.

In the second segment I will show how other properties of the locusts' behaviour may have evolved and the reasons behind their evolution.

Chapter 4

Evolutionary Game Theory

4.1 Conflicts

The best way to introduce evolutionary game theory is to consider a situation in which there is conflict between animals the result of which influences their ability to pass on their genes to the next generation of animals. This is the so-called "Darwinian struggle for survival". Although in my models I will not have conflict in the form of fighting, there will be competition for resources (food) or competition to escape a predator, which will influence the animal's ability to pass on its genes. These can be modelled by evolutionary conflict games, one of the most famous of which is the so-called 'hawk-dove' game [19].

Often in nature conflicts between animals are settled by peaceful means such as displays, rather than fights. In many cases threatening signals and assessments of strength serve to settle contests for food, territory and mates meaning that escalated fighting leading to injury or death is uncommon, but not completely absent. For example if one stag challenges another's dominant position they may well engage in a roaring match, starting slowly at first and gradually increasing the rate. If the challenger does not back down at this stage then the roaring match may be followed by a 'parallel walk'[1]. The parallel walk may end with a retreat or with a direct strength contest: the stags clash head on, interlock antlers and push against each other. If one stag turns earlier from the parallel walk and faces his opponent with the lethal points of his antlers, the first stag halts his attack and continues with the parallel walk, such is his determination to avoid escalation. Few such contests lead to serious injuries for either party. Clearly this restrained nature of animal aggression is for the good of the species, but since it was earlier demonstrated that natural selection does not act at the species level what is the explanation for this restrained behaviour from an evolutionary point of view? It is natural to think that a stag that escalates and wins fights against his rivals will inherit their mates and territory and hence multiply faster than stags with the conventional non-escalating strategy. The stag's male offspring should also inherit this behaviour and hence escalation should become the dominant trait in fights between rival stags. Why then are escalated contests so rare [19]?

For the answer, I turn to evolutionary game theory. Suppose that there are only two behavioural types: One escalates the conflict until injury or the flight of an opponent settles the issue, the other just displays as usual and retreats if an opponent starts to escalate the situation. The individuals practising these two behavioural types are known (in somewhat

[1]The two stags walk parallel to each other back and forth presumably to give a mutual display of quality which exposes of the largest profile of the body and antlers for comparison.

of a misnomer[2]) as 'hawks' and 'doves' respectively. The contest may take place over food, mates or territory. The prize for the winner corresponds to a gain in fitness G, while an injury reduces a competitors fitness by C. Fitness and success here are taken to mean (as is usual in evolutionary biology) reproductive success.

If two doves meet they will display until one of them eventually retreats. The winner obtains the gain in fitness, G, and the loser gains nothing, but it is important to note that he also loses nothing. Thus the average payoff for each participant from a 'dove-dove' encounter is $G/2$. A dove that encounters a hawk will flee with unchanged fitness, leaving the hawk to gain the full benefit G each time. Finally a hawk meeting a hawk will always result in injury to one party or the other. One individual takes the payoff G but the other individual incurs a cost C and hence the average payoff for each individual in a 'hawk-hawk' encounter is $(G-C)/2$. This average is negative if the cost of injury exceeds the prize won in the fight (which I shall always assume it does)[19]. We can summarise these results neatly in a payoff matrix:

	if it meets a hawk	if it meets a dove
A hawk receives	$\frac{G-C}{2}$	G
A dove receives	0	$\frac{G}{2}$

Table 4.1: *Payoff matrix for the 'hawk-dove' game.*

In a population mainly of doves, a hawk strategy will spread, gaining a payoff of G every time a dove is encountered in comparison to the payoff of $G/2$ for two doves meeting each other. On the other hand in a population of mostly hawks, doves will spread as the zero payoff they receive from retreating is larger than the average negative payoff, $(G-C)/2$ that is achieved for the prevalent 'hawk-hawk' encounters. Neither type of behaviour is better than the other. The success of each strategy depends on the composition of the population in which it is being played. Suppose that the frequency of the hawks in the population is x and correspondingly that of the doves is $1-x$, then for hawks the average increase in fitness will be $x(G-C)/2 + (1-x)G$: the payoff for meeting a hawk, $(G-C)/2$, multiplied by the probability of meeting a hawk in the population, x, plus the payoff for meeting a dove, G, multiplied by the probability of meeting a dove, $(1-x)$. The average increase in fitness for the dove is similarly calculated to be $(1-x)G/2$. Equality holds if and only if

$$x(G-C)/2 + (1-x)G = (1-x)G/2,$$

which implies $x = G/C$. If the frequency of hawks is less than G/C, then the fitness of the hawks will be larger than that of the doves and hence the hawks will spread and the proportion of hawks in the population will change. However, if the frequency of hawks is larger than G/C, then the doves will do better and spread into the population diminishing the hawks.

If the cost of injury is very high, hawk frequency will be small. This means, ironically, that non escalating conflicts will be prevalent in species capable of delivering the most serious injuries. On the other hand it is found that seemingly harmless real doves will fight to the death when confined to a cage [19].

[2]The conflicts are of course supposed to take place between members of the same species, furthermore it is found that doves in some circumstances do escalate.

4.2 Other Types of Game

The 'hawk-dove' game is a specific example of the general game involving two participants. The general two participant game has its origins in another specific example, the simple gambling game called prisoner's dilemma. Biologists such as W.D. Hamilton and Richard Dawkins agree that "many wild plants and animals are engaged in ceaseless games of prisoner's dilemma played out in evolutionary time"[8]. In its original, human, version, here is how the game is played. There is a 'banker' who does not take part in the game itself except to adjudicate and pay out winnings (or accept fines). Two players play 'against' each other (although, as I will show, for the benefit of the two participants, 'against' is not how should they play with each other). Both players hold two cards in their hands one labelled 'COOPERATE' and one labelled 'DEFECT'. To play one round each player chooses one of their cards to play and lays it face down on the table so that neither can be influenced by the other's move. The banker turns over the two cards and, dependent on what the cards are, distributes the winnings. Since there are two players each with two cards there are four possible outcomes to the game:

OUTCOME 1: Both players choose to cooperate. The banker pays both players a sum of money r, the *reward* for mutual cooperation.

OUTCOME 2: Both players choose to defect. The banker fines both players $-p$, the *punishment* for mutual defection.

OUTCOMES 3 and 4: One of the players chooses to defect whilst the other chooses to cooperate. The banker pays the defector a sum of money t, the *temptation* to defect and fines the cooperator a sum of money $-s$, the *sucker's* payoff.

In order for the game to remain a dilemma for the participants the temptation to defect, t, must be larger than the reward for mutual cooperation, r, otherwise there would be no temptation to defect for either player[3]. This condition is summarised as $t > r$. Also the fine for mutual defection, $-p$, should be less than the fine for cooperating when the other defects, $-s$, otherwise a false cooperation would not be punished severely enough to stop it being worth while. This condition can be summarised as $-p < -s \Rightarrow p > s$.

However, in the general cooperate-defect game, where the different payoffs will give rise to different results, there does not always have to be a temptation to defect. It is easier to see the asymmetry of the general game if seen from the point of view of the player [8]. Imagine you and I are the players. The results from one game of the general cooperate-defect game can be summarised in the payoff matrix, Table 4.2:

	if I cooperate	if I defect
If you cooperate you gain	r	s
If you defect you gain	t	p

Table 4.2: *Payoff matrix for cooperate-defect games.*

[3]The reason the game is called prisoner's dilemma as follows. Consider two thieves (or prisoners) being questioned by the police after having committed a bank robbery together. The police have insufficient evidence for a conviction. Having separated both prisoners the police visit each of them to offer the same deal: if one 'defects' and testifies for the prosecution against the other and the other 'cooperates' and remains silent, the betrayer goes free and the silent accomplice receives the full 10-year sentence. If both 'cooperate' and stay silent, both prisoners are sentenced to only six months in jail for a minor charge. If each 'defects' and betrays the other, each receives a five-year sentence.

In order to analyse the game better, carry out the simple transformation of subtracting p and dividing through by $r - p$ to give the new normalised payoff matrix Table 4.3:

	if I cooperate	if I defect
If you cooperate you gain	1	S
If you defect you gain	T	0

Table 4.3: *Normalised payoff matrix for cooperate-defect games.*

Here $S = (s - p)/(r - p)$ and $T = (t - p)/(r - p)$. It is far easier to see now that for the game to represent prisoner's dilemma $T > 1$ and $S < 0$, which are equivalent to the previous conditions $t > r$ and $s < p$, (provided the reward for mutual cooperation, r is greater than the punishment for mutual defection, p, which in the case of prisoner's dilemma it must be). There are three other types of game that are exhibited from the general coop-defect game. The 'hawk-dove' game which I have already introduced occurs if $S > 0$ and $T > 1$. There is a third game called (ironically given the example given above for the 'hawk-dove' game) 'the stag hunt'. The hypothetical situation is as follows. Two acquaintances go out hunting. They have two possible ways to spend their time and ammunition. They can both cooperate and try to hunt a stag for which there will be a large payoff, but at the same time a large risk for each if his fellow hunter lets him down. If one hunter defects and decides to play it safe by catching a hare, then the other will have a very hard time trying to catch a stag on his own. On the other hand he too may play it safe and try to catch a hare as well. The normalised form of the game occurs if $T < 1$ and $S < 0$. The final game, which occurs if $S > 0$ and $T < 1$, is called 'harmony'. Essentially this is quite a boring game. There is no temptation to defect and in its iterated version (played several times over) it should end with both players cooperating every time for reasons demonstrated later in Section 4.8.

4.3 Evolutionary Stability

Now we have dealt with an example of a simple game we can consider the concept of evolutionary stability. A type of behaviour is said to be *evolutionarily stable* if, whenever all members of the population adopt it, no dissident behaviour can invade the population under the influence of natural selection [19].

To formalise this idea, consider two types of individual I and J (hawks and doves for example). Denote $W(I, Q)$ as the fitness of an individual of type I in a population of composition Q, and by $xJ + (1-x)I$ denote the mixed population where x is the frequency of J-types and $(1 - x)$ that of I-types. A population consisting of I-types will be *evolutionarily stable* if whenever a small amount of deviant J-types are introduced, the common type I fares better than the newcomers J. This means that for all $J \neq I$

$$W(J, \varepsilon J + (1 - \varepsilon)I) < W(I, \varepsilon J + (1 - \varepsilon)I) \tag{4.3.1}$$

for all sufficiently small $\varepsilon > 0$. We assume that the population is large enough that $W(I, Q)$ is continuous in the second variable. This means that a small change in the composition of the population will have only a slight effect on the fitness of I. By letting $\varepsilon \to 0$, (4.3.1) gives

$$W(J, I) \leq W(I, I) \tag{4.3.2}$$

for all J. This means that no type fares better against a population of I-types than an I-type itself. In the hawk dove game neither of the two behavioural types on its own is evolutionarily stable as each one can be invaded by the other. Behaviour that consists of escalating with probability $p = G/C$ cannot be invaded by another type and hence is evolutionarily stable strategy (ESS). This sort of strategy is known as a mixed strategy, where hawk behaviour is exhibited with a certain probability and dove with another probability [19].

4.4 Nash Equilibria

When generalising the idea of the mixed strategy as introduced above, assume that the behaviour used by each 'player' can be described in terms of a finite set of pure strategies. A pure strategy is a strategy in which a certain type of behaviour (hawk or dove for example) is played with probability one. In general assume that there are N such pure strategies R_1 to R_N, and that the players are also allowed to use mixed strategies: these will consist of playing the pure strategies, R_1 to R_N, with certain predetermined probabilities, p_1 to p_N. A strategy, denoted $\mathbf{p} = (p_1, \ldots, p_N) \in \mathbb{R}^N$ is clearly a pure strategy if $p_i = 1$ for some i and $p_j = 0$ for all $j \neq i$.

Assume, at first, that the game involves only two players, and denote by u_{ij} the payoff for a player using the pure strategy R_i against strategy R_j. The $N \times N$ matrix $\mathbf{U} = (u_{ij})$ is said to be the payoff matrix, the generalisation of Table 4.2. An individual using the R_i strategy obtains an expected payoff $(\mathbf{Uq})_i$ against the $\mathbf{q}$ strategist (since q_j is the probability that he is met with strategy R_j). The payoff for a $\mathbf{p}$ strategist against a $\mathbf{q}$ strategist is, therefore, given by

$$\mathbf{pUq} = \sum_{i,j} u_{ij} p_i q_j \tag{4.4.1}$$

A best reply to strategy $\mathbf{q}$ is a strategy $\mathbf{p}$ for which the map $\mathbf{p} \to \mathbf{pUq}$ attains its maximal value. The set of best replies must contain at least one pure strategy.

The most important notion in game theory is that of a Nash equilibrium: a strategy which is a best reply to itself. A strategy $\mathbf{q}$ is said to be a strict Nash equilibrium if it is the *unique* best reply to $\mathbf{q}$, i.e. if

$$\mathbf{p} \cdot \mathbf{Uq} < \mathbf{q} \cdot \mathbf{Uq} \tag{4.4.2}$$

holds for all strategies $\mathbf{p} \neq \mathbf{q}$ [19]. A strict Nash equilibrium must be a pure strategy [19].

4.5 Evolutionarily Stable Strategies

Consider a large population of players who encounter randomly chosen opponents. If all the players use the same strict Nash equilibrium then every individual deviating from it will be penalised, hence such deviation will not spread. In the 'hawk-dove' game it has been shown there is no strict Nash equilibrium. It cannot be assumed that every non-strict Nash equilibrium is non-invadable by a dissident minority. The invaders may use a strategy which does just as well and may spread, unless the dissidents encounter an evolutionarily stable population.

Recalling the definition of evolutionary stability as given in (4.3.1) with the two 'types' I and J replaced by two strategies $\hat{\mathbf{p}}$ and $\mathbf{p}$ and the population $\varepsilon J + (1 - \varepsilon)I$ replaced by the

strategy mix $\varepsilon\mathbf{p} + (1-\varepsilon)\hat{\mathbf{p}}$. Thus the strategy $\hat{\mathbf{p}}$ will be said to be *evolutionarily stable* if for all strategies $\mathbf{p}$, with $\mathbf{p} \neq \hat{\mathbf{p}}$, the inequality

$$\mathbf{p} \cdot \mathbf{U}(\varepsilon\mathbf{p} + (1-\varepsilon)\hat{\mathbf{p}}) < \hat{\mathbf{p}} \cdot \mathbf{U}(\varepsilon\mathbf{p} + (1-\varepsilon)\hat{\mathbf{p}}) \tag{4.5.1}$$

holds for all $\varepsilon > 0$ that are sufficiently small, i.e. smaller than some appropriate *invasion barrier* $\bar{\varepsilon}(\mathbf{p})$. This basically says that the strategy $\hat{\mathbf{p}}$ will do better against a population mainly of strategy $\hat{\mathbf{p}}$ invaded by a small amount of strategy $\mathbf{p}$ than the invading strategy $\mathbf{p}$ itself does against this invaded population. This means that even if $\mathbf{p}$ finds itself in the population it will not be able to gain a foothold and will be quickly wiped out.

By a simple rearrangement equation (4.5.1) can be re-written as

$$(1-\varepsilon)(\hat{\mathbf{p}} \cdot \mathbf{U}\hat{\mathbf{p}} - \mathbf{p} \cdot \mathbf{U}\hat{\mathbf{p}}) + \varepsilon(\hat{\mathbf{p}} \cdot \mathbf{U}\mathbf{p} - \mathbf{p} \cdot \mathbf{U}\mathbf{p}) > 0 \tag{4.5.2}$$

This implies that $\hat{\mathbf{p}}$ is an ESS if and only if the following two conditions are satisfied:

1. *equilibrium condition*

$$\hat{\mathbf{p}} \cdot \mathbf{U}\hat{\mathbf{p}} \geq \mathbf{p} \cdot \mathbf{U}\hat{\mathbf{p}} \text{ for all possible } \mathbf{p},$$

2. *stability condition*

$$\text{if } \mathbf{p} \neq \hat{\mathbf{p}} \text{ and } \hat{\mathbf{p}} \cdot \mathbf{U}\hat{\mathbf{p}} = \mathbf{p} \cdot \mathbf{U}\hat{\mathbf{p}}, \text{ then } \mathbf{p} \cdot \mathbf{U}\mathbf{p} < \hat{\mathbf{p}} \cdot \mathbf{U}\mathbf{p}.$$

Condition (1) is simply the definition of a Nash equilibrium: Strategy $\hat{\mathbf{p}}$ is a best reply against itself. However, this property alone does not guarantee non-invadability, since it allows the potential existence of another strategy $\mathbf{p}$ which is an alternative best reply. the stability condition states that, in such a case, $\hat{\mathbf{p}}$ fares better against $\mathbf{p}$ than $\mathbf{p}$ itself. Hence a strict Nash equilibrium implies an ESS and conversely an ESS implies a Nash equilibrium [19].

4.6 The Replicator Equation

In certain situations, the underlying dynamics of evolutionary stability can be modelled by an ODE. Thus assume that the population is divided into n types[4] E_1 to E_n with respective frequencies x_1 to x_n. The fitness f_i of E_i will be a function of the composition of the population, i.e. of the state $\mathbf{x} = (x_1, \ldots, x_n)$. If the population is very large and if generations blend continuously into each other, it may be assumed that the state $\mathbf{x}$ evolves as a differentiable function of t. The rate of increase $\frac{dx_i}{dt}/x_i$ of type E_i is a measure of its evolutionary success. If a type E_i which has a small initial frequency x_i is increasing at the same rate as a type E_j which has a large initial frequency x_j then clearly in terms of evolutionary success type E_i is doing better than type E_j. This is reflected in $\frac{dx_i}{dt}/x_i$. Similarly this measure of evolutionary success distinguishes between two types with the same initial frequency increasing at different rates, clearly the one increasing at the fastest rate will be the more successful in an evolutionary context. Following the basic tenet of Darwinism, namely natural selection, this success can be expressed as the difference between fitness,

[4]For the sake of generality I will switch to denoting fitness as f_i for a population type that will now be denoted E_i

$f_i(\mathbf{x})$, of E_i and the average fitness, $\bar{f}(\mathbf{x}) = \sum x_i f_i(\mathbf{x})$, of the population. Formulating this mathematically gives

$$\frac{dx_i}{dt}/x_i = \text{fitness of } E_i \;-\; \text{average fitness},$$

which gives the replicator equation [19]:

$$\frac{dx_i}{dt} = x_i(f_i(\mathbf{x}) - \bar{f}(\mathbf{x})) \text{ for } i = 1, \ldots, n. \tag{4.6.1}$$

It should be noted that (4.6.1) was derived assuming that the success of E_i corresponds to its rate of increase and tacitly that inheritance is both asexual and without mutation.

4.7 Other Types of Game Revisited

Recall the normalised payoff matrix for the general 2×2 cooperate-defect game.

	if I cooperate	if I defect
If you cooperate you gain	1	S
If you defect you gain	T	0

Table 4.4: *Normalised payoff matrix for the general cooperate-defect game.*

Assume, as in the hawk dove game, there is mixture of the two strategy types, cooperate and defect, in the population. Let x be the frequency of cooperators in the population and consequently $1 - x$ is the frequency of defectors. In a similar manner to before the average increase in fitness for a cooperator is $P_C = x + (1 - x)S$ and the average fitness increase for being a defector is $P_D = Tx$. Now the average payoff for the whole group of cooperators and defectors is $P_A = xP_C + (1 - x)P_D = x^2(1 - S - T) + x(S + T)$. Applying the replicator equation (4.6.1) from Section 4.6 to the general 2×2 normalised game gives

$$\begin{aligned} \frac{dx}{dt} &= x(P_C - P_A) \\ &= x(x(1 - S) + S - x^2(1 - S - T) - x(S + T)) \\ &= x(1 - x)(S - x(S + T - 1)). \end{aligned} \tag{4.7.1}$$

Letting $\frac{dx}{dt} = 0$ on the right hand side of the above differential equation gives the steady states of the system. There are stationary points at $x = 0$, $x = 1$ and $x = \frac{S}{S+T-1}$ provided $0 < \frac{S}{S+T-1} < 1$. (If $\frac{S}{S+T-1} < 0$ or $\frac{S}{S+T-1} > 1$ there is of course still a fixed point at $x = \frac{S}{S+T-1}$ but it has no physical meaning as the proportion of the population that are cooperators cannot be less than zero or greater than one). So it is the values of S and T that determine the nature and position of the fixed points. By simple analysis of the above differential equation it can be shown that there are four distinct possibilities of combinations of S and T which give different qualitative behaviour as far as evolutionarily steady states are concerned.

If $S > 0$ and $T < 1$ then there is a stable steady state at $x = 1$ and an unstable steady state at $x = 0$ implying that cooperation will dominate the population (see Figure 4.1 (A) overleaf). This is the game referred to earlier as 'harmony'.

If $S > 0$ and $T > 1$ then there are unstable steady states at $x = 0$ and $x = 1$ and since $0 < \frac{S}{S+T-1} < 1$ a stable steady state at $x = \frac{S}{S+T-1}$. This situation is equivalent to the hawk-dove game (see Figure 4.1 (B)).

If $S < 0$ and $T > 1$, there is an unstable steady state at $x = 1$ and a stable steady state at $x = 0$ implying that defectors will dominate the population at the expense of cooperators, who will die out. This is equivalent to the game of prisoner's dilemma (see fig 4.1 (C)).

Finally if $S < 0$ and $T < 1$ again there is a steady state at $x = \frac{S}{S+T-1}$ as well as at $x = 0$ and $x = 1$, however, this time $x = 0$ and $x = 1$ are both stable and $x = \frac{S}{S+T-1}$ is unstable. Which of the two stable steady states the population will evolve to depends on the initial conditions, (see Figure 4.1 (D)). This game is equivalent to 'the stag hunt' situation.

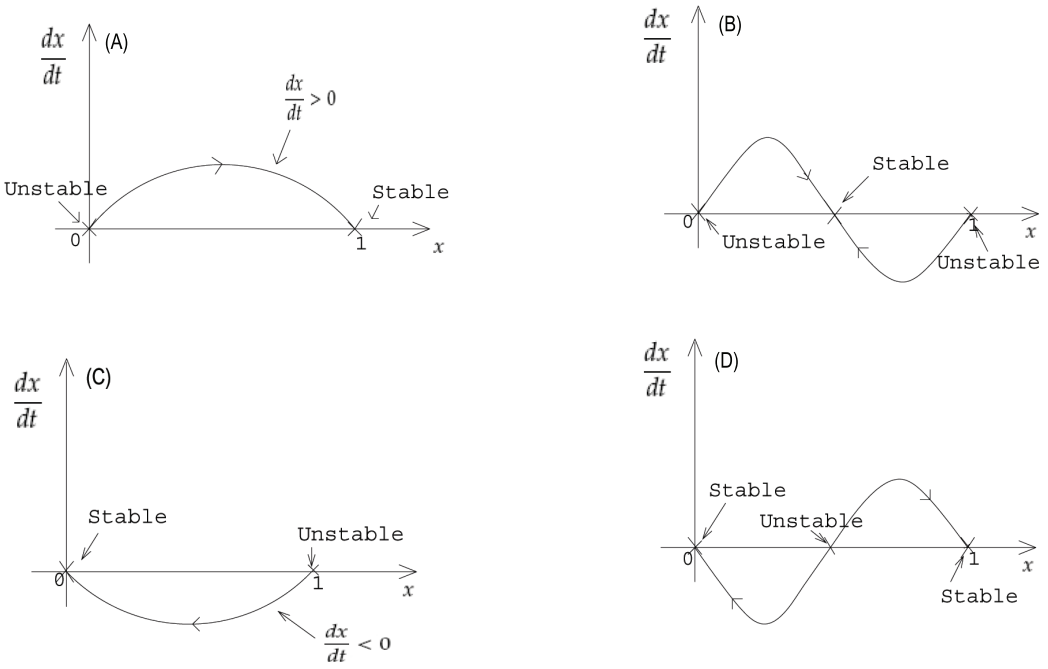


Figure 4.1: *The four different qualitative behaviours of the cooperate defect game. The x axes represent the proportion of cooperators in the population. The stable fixed points on the above diagram correspond to evolutionarily stable strategies (see Section 4.5)*

4.8 Optimal Strategy Versus Evolutionarily Stable Strategy

It is important to emphasise the difference between an optimal strategy and an evolutionarily stable strategy. For example in the game of prisoner's dilemma, the optimal strategy for both parties to cooperate. This way they both get the maximum individual payoff, which corresponds to the maximum average payoff. However, if the temptation to defect is great enough, although defecting will not give an individual a higher payoff, it will give him a comparatively higher payoff with respect to his fellow participant. Natural selection will act to favour the player with the higher payoff, even if this payoff is lower than the highest achievable. It is therefore in the interests of a player to defect if the other cooperates to give himself a comparatively higher payoff. This will mean that the risk of cooperating will be to great so both players will end up defecting. In this case either player who spontaneously

decides to cooperate will be penalised with a comparatively lower pay off and will not be favoured in an evolutionary sense. This means that defection will be the evolutionarily stable strategy, despite not being giving the optimal average payoff. This distinction will be very important in the next chapter.

Chapter 5

Two-Dimensional Model

It is in two dimensions that I will model and evolve certain properties of self-propelled particles in an attempt to recreate realistically the behaviour of animals. Animals that can be modelled using self-propelled particles include fish, swarming insects and mammals that travel in groups. As evidenced in Chapter 3, SPP models in one dimension are realistic and can give useful results. I hope to achieve the same applicability for SPP models in two dimensions by applying evolutionary game theory to the models.

I will model self-propelled particles in two dimensions using a model similar to that of Vicsek et al [26]. Consider N off-lattice particles, indexed by i, in a square cell, $L \times L$, with periodic boundary conditions. The particles will initially be given the simplest initial conditions: a random direction, θ_i and position, (x_i, y_i), with all particles having the same constant absolute velocity $u = 0.03$ as in [26]. The position of the ith particle is updated according to the following rule:

$$\mathbf{x}_i(t + \Delta t) = \mathbf{x}_i(t) + \mathbf{v}_i(t)\Delta t, \tag{5.0.1}$$

where I chose the time unit $\Delta t = 1$. The updated velocity for each particle $v_i(t + \Delta t)$ is constructed to have absolute velocity u and direction given by the angle $\theta_i(t + \Delta t)$. This angle is updated according to the rule:

$$\theta_i(t + \Delta t) = \theta_i(t) + \Delta t \left(arg \left[\exp \left(\mathbb{i} \sum_{j \in \mathcal{J}_i^r} \theta_j(t) + \mathbb{i} \Delta Q \right) \right] - \theta_i(t) \right), \tag{5.0.2}$$

where $\mathcal{J}_i^r \equiv \mathcal{J}_i^r(t)$ is the set of all $j \in 1, 2, \ldots, N$ such that $\|\mathbf{x}_i(t) - \mathbf{x}_j(t)\|_2 \leq r$, i.e. all particles that are in the two dimensional interaction neighbourhood of the ith particle. $\mathbb{i} = \sqrt{-1}$ and ΔQ is a random number[1] from the uniform distribution $Q(x)$ (as given on page 29), where this time I chose the width of the interval to be $\xi = 2$ and nondimensionalised density of $\rho = \frac{80}{25^2} = 0.128$ particles per unit length squared. These parameter values were chosen empirically after initial tests of the code to give a phase transition for varying IR, r, of order 1.

[1] It should be noted that for the two dimensional model I have decided to implement the noise in the manner of Gregóire and Chaté [15]: As opposed to making an error when trying to take the direction they have 'perfectly' calculated ('angular noise') particles make errors when estimating the neighbouring velocities. This seems to be a more realistic model for locusts in two dimensions.

5.1 Optimal Radius for Following the Leader

In two dimensions, in order to be able to evolve the IR of the particles realistically, I will need to consider a second sort of alignment, other than the alignment $\zeta_{overall}$ defined in Chapter 3. For this new alignment I will introduce the concept of a leader particle. The leader particle, as described in [21] and [6], is an informed individual particle which is unaffected by the others, whereas all the other particles can be influenced by the leader and each other. In reality, this particle represents an individual who has seen something (like an item of food or a predator) that others have not and that moves towards this item of food or away from the predator without deviating from his path. In reality if a predator is detected by an individual his actions can lead the group away to safety or if food is spotted the leader can take the group towards the food. In such cases it is clearly to the advantage of the rest of the individuals in the group to follow the leader towards the food or away from the predator. Hence, the other type of alignment I consider is alignment to the leader particle, or 'direction specific alignment', ζ, calculated for each particle.

Without loss of generality the leader particle will be made to travel at and angle of $-\frac{\pi}{4}$ to the x-axis. In order to get a good measure of how well a particle has followed the leader consider the difference between the leader's displacement from its initial position and each particle's displacement from its original position. The square of the magnitude of the difference between the two displacements will become the fitness value, the basis on which selection will take place. Alignment to the leader for the ith particle is averaged over the whole of the simulation and given by

$$\zeta_i = 1 - \frac{1}{(2J)^2}\left[\left(\sum_{j=1}^{J}\cos(\theta_i(t_j)) - J\cos(-\pi/4)\right)^2 + \left(\sum_{j=1}^{J}\sin(\theta_i(t_j)) - J\sin(-\pi/4)\right)^2\right]. \quad (5.1.1)$$

The reason average alignment to the leader over all the time is used rather than just the second half of the simulation (as was considered when looking at the alignment in the one dimensional model) is to make the model more realistic. In nature animals will not necessarily be given time to align themselves with the leader before they are eaten by a predator[2].

Direction specific alignment will become the particle's fitness value, the basis on which the particle is selected to pass on its characteristics to the next generation. The particles that spend the largest amount of time going in the same direction as the leader will be, in reality, the animals that would eat more food or be more likely to escape predation, so in my model will be the particles that are most likely pass on their characteristics to the next generation. In this way I hope to mimic natural selection, the driving force behind evolution.

The way I will model reproduction is initially by assuming it is purely asexual with no overlapping generations and a constant population, which, although unrealistic, has been found to give surprisingly good results [19]. Also initially assume that there is no mutation of the evolved characteristic between generations. When the simulation is run

[2]It is possible that as an extension to the project the particles could be allowed to align ('warm up'[27]) for a certain period of time before the introduction of the leader as this may be the more realistic situation in nature when a food item is first spotted. I would argue, however, that in the case of the arrival of a predator, it is more likely that the animals will be aggregated, possibly not moving (i.e. feeding or resting) and very probably facing in random directions when the predator is first spotted. Therefore modelling the animals with random initial conditions and a leader particle from the start is not unrealistic.

for one generation, each particle $i = 1, 2, \ldots, N$ will be assigned a fitness, f_i, according to how well it followed the leader during its life span. The strength of selection is then chosen using the formula

$$\hat{f_i} = \frac{1 - w + w f_i}{N(1-w) + w \sum_{i=1}^{N} f_i}, \tag{5.1.2}$$

for $0 < w < 1$, which also normalises the fitnesses so that $\sum_{i=1}^{N} \hat{f_i} = 1$. Choosing $w = 1$ is known as strong selection; clearly the fitnesses are just normalised and left with their relative magnitudes unchanged. Choosing $w \ll 1$ is known as weak selection as the differences between the fitnesses of the particles are emphasised less; in the extreme $w = 0$, the original fitnesses, f_i, are ignored and all particles end up with the same fitness $\hat{f_i} = \frac{1}{N}$. During this project strong selection, $w = 1$, will be used as the effect of using weak selection seems to be to achieve the same results only taking a longer time.

In nature it is usual that the animal that displays the strongest phenotype will pass his genes on to the largest proportion of the population, however it sometimes happens that either the fittest animal may die prematurely before fulfilling his reproductive potential or that for some reason the phenotype of the child will not match that of the parent (perhaps due to some illness as an infant). This selection technique is an attempt to mimic natural selection as closely as possible (within certain bounds of complexity), by adding some element of randomness to the process to allow for situations described above. Thus the normalised fitness of each particle (dropping the ˆ) can be considered to take up a space of length f_i in the unit line segment with f_1 at the left hand extreme and f_N at the right hand extreme. Then for each of the N particles in the new generation choose a random number from the uniform distribution between 0 and 1. The new particle will take its characteristics from the particle whose fitness covers the segment in which the corresponding random number lies. This is equivalent to saying that each particle's characteristics are passed onto the next generation of particles with probability

$$p_i = f_i. \tag{5.1.3}$$

This method neatly avoids the problem of having to divide up the N new generation particles between fitnesses that are unlikely to give integers when multiplied by N. Once the new generation of particle has been created with the characteristics inherited from the previous generation the process is restarted.

There are several possible characteristics of the particles that could be evolved. For example in their paper, [27], Wood and Ackland consider characteristics of self-propelled particles such as radius of attraction, radius of repulsion, radius of alignment, angle of interaction (modelling the blind spot of the animals). They also have a compromise between size of IR and angle of interaction as well as the speed of a particle and its turning ability, which seem quite realistic biologically, i.e. the faster an animal moves the slower it will be at turning. In this project a possible trade off is between IR and particle speed so that particles do not become infinitely far sighted which is clearly not biologically realistic. I will, however, try to avoid adding in a trade off in order to better understand the underlying dynamics of the model: adding a trade off will only make the model more complicated than is necessary to exhibit evolutionary dynamics. For similar reasons I will also not consider the evolution of parameters such as radius of repulsion and radius of attraction as my

model does not have these features built in. The shape of the interaction neighbourhood will also be fixed as a circle (in two dimensions), so the particles are not considered to have a blind spot[3]. The parameter that I will evolve will be the IR, initially with no constraint with regards to the speed of particle movement.

As well as varying r I again considered whether the weighting the particle gives to its own direction compared to that of the measured directions of its neighbours had an effect on the alignment of the particles. The new angular update equation is given by

$$\theta_i(t+\Delta t) = \theta_i(t)+\Delta t\left\{arg\left[\exp\left(\frac{\mathbb{i}\alpha\theta_i(t)}{n+\alpha}+\frac{\mathbb{i}}{n+\alpha}\left\{\sum_{j\in\mathcal{J}_i^r}\theta_j(t)-\theta_i(t)\right\}+\mathbb{i}\Delta Q\right)\right]-\theta_i(t)\right\}, \quad (5.1.4)$$

where n is the number of neighbours of the ith particle, excluding itself. Choosing $\alpha = 1$ and $\Delta t = 1$ in (5.1.4) gives an angular update equation where all the neighbouring particles (including particle i itself) are given equal weighting as in (5.0.2). As in the one dimensional case, when plotting the alignments with varying values of α and r, I found that even varying α between 0 and 5 had very little effect on the overall alignment of the particles (see Figure 5.1 (A), (B) and (D)[4] page 54). This independence of α, a property shared by both alignment and alignment to the leader, is a result that has not been documented before. The result enabled me to keep the weighting parameter fixed at $\alpha = 1$, without loss of generality, (i.e. all the particles are given equal weighting) and to vary only r, the IR, making the model more efficient.

There is little difference between Figure 5.1 (A) displaying the alignment of a group without a leader and Figure 5.1 (B) displaying the alignment of a group with a leader. This means that simple alignment will not be a good selection criterion for evolution with a leader, as it is seemingly independent of the leader's presence. Figure 5.1 (C) displays the alignment to what would be the leader's direction, if there were a leader, for a group of particles where no leader was present. As expected the alignment to the leader is low. Figure (D) shows the alignment to the leader when the leader was present. It can be seen that qualitatively the surface looks similar to (A) and (B) (for simple alignment), with alignment to the leader increasing when all the particle have the same large IR. This means particles will follow the leader more when they have larger IR indicating that IR would be a good parameter to use for selection [5].

Clearly the optimal IR is a large one giving all the particles the maximum payoff, which clearly leads to the maximum average payoff for the whole group. A large IR is equivalent to the cooperate strategy discussed in Section (4.8): it will give the maximum average

[3]Clearly as far as sight goes this is unrealistic, but animals can sense things behind them using senses other than sight. For example crickets and locusts are at risk of being eaten (for their protein and salt content)[22] by fellow members of a marching band if they stand still for too long. This stimulus from behind is a large factor in making the locusts move forwards. It was found in an experiment by Bazazi et al [3] that when the locusts hind legs were anaesthetised that the locusts ceased to move forwards and in fact had their hind legs eaten by locusts marching behind.

[4]These figures have a nearly uniform cross section indicating that the alignment varies very little with changing α, but varies a lot as r goes from 0 to 10. This is sufficient justification for keeping α, the weighting parameter, constant.

[5]The alignments in figures (A) and (B) vary over a much larger range than in figures (C) and (D). This is because of the way I have defined the alignment to the leader. It is unlikely that there will be alignment values near zero for figures (C) and (D) as this would involve all the particles travelling in the opposite direction to the leader all the time, which is unlikely even when no leader is present. It is not particularly important how large the range of alignments is as selection is carried out using relative alignments.

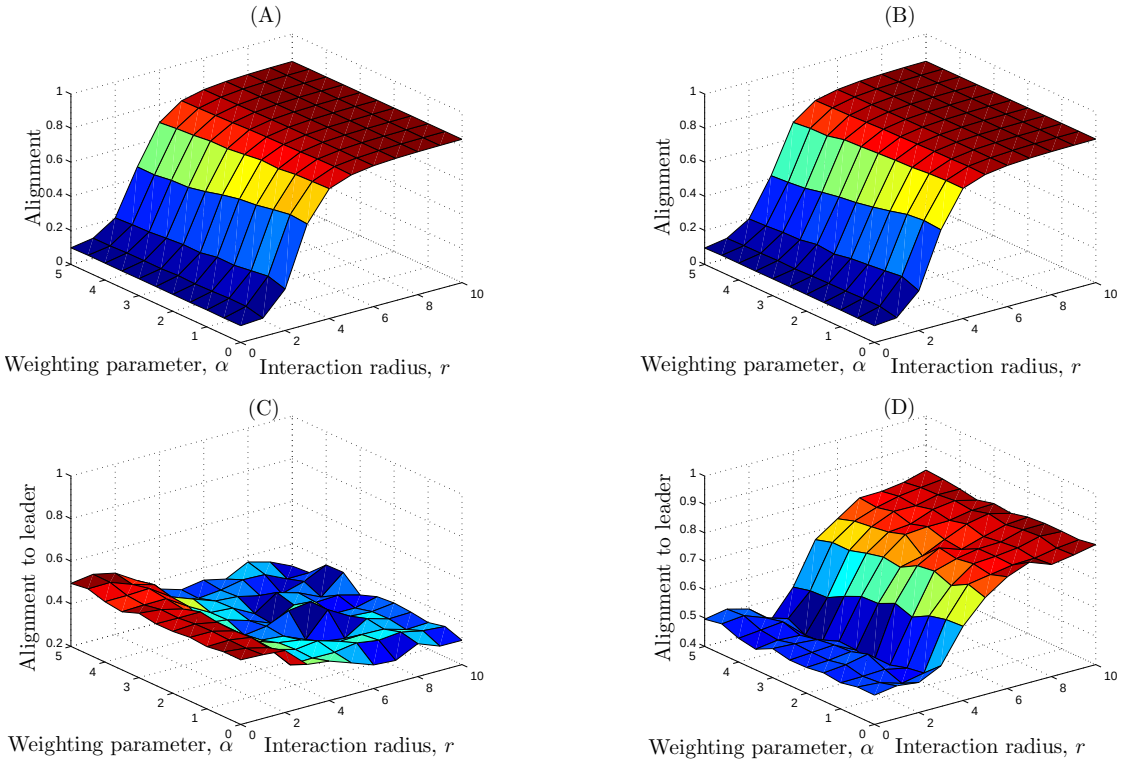


Figure 5.1: *Varying alignments of the particles in the two dimensional model plotted as a surface for varying r and α with noise parameter $\eta = 2$, population size $N = 80$ and domain size $L = 25$. The 2-D code was run for $121 (= 11^2)$ different combinations of r and α over 500 timesteps and the alignments over all 500 timsesteps were measured. This was then repeated 50 times and the alignments averaged and plotted as surface. Figure (A): Alignment of a group without a leader. Figure (B):Alignment of a group with a leader. Figure (C): Alignment to what would be the leader's direction, if there were a leader, for a group of particles where no leader was present. Figure (D): Alignment to the leader when the leader was present. The code used to find the behaviour displayed in (A) and (C) was* `vicsekspacerepeat.m` *and the code used to find the behaviour in (B) and (D) was* `vicsekleaderspacerepeat.m`.

payoff, but it will not necessarily be the evolutionarily strategy favoured by each particle. If one particle can do better than the others by defecting from this strategy (using a small IR) then it will be favoured by evolution and this defecting strategy will become more prevalent in the population.

5.2 Investigation into The Evolutionarily Stable Radius for Following the Leader

In order to test evolutionary stability of a strategy[6] (see Section 4.3) I will run what is known as an 'invasion test'. It tests the stability of population made up almost entirely (proportion $1 - \varepsilon$) of type I against a small amount (ε) of deviant type, J. The code `vicsekleaderrepeatevolutioninvasion.m` simulates N SPPs, $N-1$ of which with one IR and 1 with a another (i.e. $\varepsilon = 1/N$). It will run the particles for one simulation and then evolve them in the manner described in Section 5.1. It repeats this process until one of the

[6]For convenience, I will consider only pure strategies (i.e. all the particles have the same interaction radius).

two IR completely dominates the population, i.e. all the particles have the same IR. This whole process is repeated N times. A strategy is said to be invasive if starting as the lone particle it comes to dominate the population for more than or equal to $\varepsilon = \frac{1}{N}$ of the repeats. Here the term dominate means to completely wipe out the other type of particle. This is the test of evolutionary stability: if a population mainly of type I individuals is not invaded by any of the other types of individual, J, that try to invade, over all of the N repeats then the strategy of all type I particles is considered to be an ESS.

In an ideal world I would like to try mixed strategies against each other, but due to the computationally intensive nature of the code and the infinity of possibilities for a mixed strategy, I will have to limit the experiment to pure strategies, accepting the possibility that none of these will be an ESS. Also I would like to do more than N repeats and take an average to get a clear idea of invasion, but since each evolutionary process is so computationally intensive, I am restricted to only N repeats. This should, however, still give a good idea of the stability of a strategy. Similarly I would like to be able to test many different radii against each other (given that length is of course a continuous variable) and find out which invades the other. However, this is not possible, so at first I will try a large range of IR over which the phase change occurs in Figure 5.1 (D). This range of IR will be known as the coarse experiment. When the range in which the dominant IR lies has been found, the range of interaction radii can be refined and the experiment rerun with smaller intervals between a smaller range of IR, the fine experiment (see Appendix B). The results of the coarse experiment are displayed below:

		1 particle						
	Interaction radius	0	1	2	3	4	5	6
79 particles	0	-	$\frac{0}{80}$	$\frac{0}{80}$	$\frac{2}{80}$	$\frac{0}{80}$	$\frac{0}{80}$	$\frac{0}{80}$
	1	$\frac{0}{80}$	-	$\frac{0}{80}$	$\frac{0}{80}$	$\frac{0}{80}$	$\frac{0}{80}$	$\frac{0}{80}$
	2	$\frac{0}{80}$	$\frac{2}{80}$	-	$\frac{0}{80}$	$\frac{0}{80}$	$\frac{0}{80}$	$\frac{0}{80}$
	3	$\frac{2}{80}$	$\frac{2}{80}$	$\frac{5}{80}$	-	$\frac{0}{80}$	$\frac{0}{80}$	$\frac{0}{80}$
	4	$\frac{8}{80}$	$\frac{5}{80}$	$\frac{4}{80}$	$\frac{4}{80}$	-	$\frac{2}{80}$	$\frac{0}{80}$
	5	$\frac{18}{80}$	$\frac{5}{80}$	$\frac{0}{80}$	$\frac{6}{80}$	$\frac{0}{80}$	-	$\frac{3}{80}$
	6	$\frac{8}{80}$	$\frac{19}{80}$	$\frac{1}{80}$	$\frac{0}{80}$	$\frac{1}{80}$	$\frac{0}{80}$	-

Table 5.1: *A table to demonstrate strategy invasion over a large range of IR. The vertical column is the IR of the particles which started with 79 particles and the horizontal row indicates the IR of particles which started with just 1 particle. The code used to carry out the invasion of each strategy was* `vicsekleaderrepeatevolutioninvasion.m`

At first the findings from the coarse experiment may seem quite counter-intuitive especially given the evidence of Figure 5.1 (D). When all the particles have the same interaction radius (IR), it is clear that, in terms of fitness, particles with a large IR (i.e. $r = 6$) outperform those with smaller IR quite substantially. Why then does it appear that particles with large IR lose out to smaller ones when the sizes of the IR are mixed? Large IR, are invaded by smaller ones far more often than the other way round, indeed, IR $r = 4$, 5 and 6 never invade IR, $r \leq 3$. It appears that if the ESS is to be pure, that it will be a strategy with a small IR giving all the particles a relatively low payoff, in comparison to the payoff each particle receives in the strategy when all the IR are large.

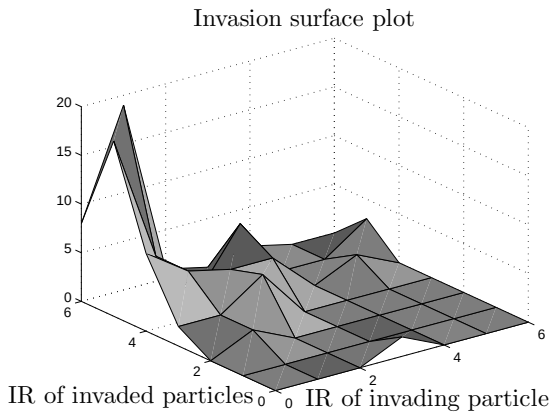


Figure 5.2: *A surface plot to show pictorially the values of the number of successful invasions when one interaction radius attempts to invade the majority of another.*

In order to understand this counter-intuitive phenomenon I used the Matlab codes `vicsekleadermovie.m` and `makemovie.m` to create movies[7]. The composition of the particles in the movies were (1) all particles with the same large IR ($r = 6$), (2) all particles with the same small IR ($r = 1$) and (3) half the particles with large ($r = 6$) and half the particles with small ($r = 1$) IR.

In situation (1) almost all of the particles follow roughly in the direction of the leader almost all of the time; the particles seem to travel as one large group. This is clearly evidenced in Figure 5.1 (B) and (D): The alignment value is high (implying that the particles travel in a large group) and the alignment to the leader is high (implying that the group of particles travel in the general direction of the leader). All the particles are cooperating with each other to achieve a higher fitness value for all.

In (2), where all the particles have small IR, most of the time the particles do not follow the leader at all. They seem to move about in small groups of twos or threes or as individuals. A particle will follow the leader for a short period of time if the two particles come into close enough proximity, which is not very often. Again Figures 5.1 (B) and (D) corroborate these findings; alignment is low indicating that the particles do not travel as a large group and alignment to the leader is also low indicating that the particles are seemingly defecting and hence all getting a lower payoff.

Finally in (3), when there is a half and half mix of particles with small and large IR, the particles with small IR move about randomly staying in approximately the same place. However, occasionally, when the leader particle passes by they will travel in the right direction for a short period of time. On the other hand the particles with large IR, tend to form groups whose overall displacement (at the end of the simulation) is large, occasionally coercing a few particles with smaller IR to join them. This group behaviour that was rewarded in (1) is now punished. There are so many particles around them in their large IR, most of them travelling in random directions, that although they travel in groups, the groups are almost never travelling in the same direction as the leader. Even when the leader passes through such a group, since it will be just one of many particles in the IR, it can pass through virtually unnoticed by a large group of large IR particles. This is

[7]The movies of the particles with three different compositions of initial IR are included in the CD accompanying this project. However, it is not necessary to see the videos in order to follow the reasoning.

a crucial difference between the two strategies. When the leader particle passes a particle with small IR it is likely that the particle has no others in its IR and is free to follow the leader. This is not true of large IR particles. A strategy which makes the particle follow the leader, even if it is just for a short time, should always do better than a strategy in which the leader particle is ignored and the particles travel in random directions.

It appears that the particles are involved in a game of prisoner's dilemma during each simulation. Although it is best for all the particles if they all 'cooperate' and use the same large IR, there is always the temptation to exploit the particles who are using a large IR, by 'defecting' and using a small IR. This way the 'defecting' particle gains on his fellows by making them do worse than him, rather than making himself do better than the rest. Since evolution is only dependent on the comparative fitnesses of the particles, the results are, practically, the same. Table 5.1 indicates that smaller IR will invade larger IR but not the other way around. We can draw a comparison here with figure 4.1 (C), which illustrates the evolutionary stability of the game of prisoner's dilemma. Cooperating is analogous to using a large IR and over time we see from the invasion matrix table 5.1, that this is an unstable steady state. A small proportion of particles deviating from the steady state cause the population to evolve away from large IR and towards small a steady state with IR, exactly as in figure 4.1 (C).

Chapter 6

Conclusions

In the first segment (Chapter 2) I introduced stochastic differential equations in a practical way, in order that they might be exploited in my modelling. Through examples I was able to introduce the basic theory behind SDEs and to recreate qualitatively the experimental switching behaviour of the alignment found in locusts. Using this SDE example I was able to apply analytical techniques in the hope they might also be applicable to the experimental situation. I introduced the Fokker-Planck equation which was used to find the stationary probability distribution of the alignment and I compared this to the stationary probability distribution found by running the SDE for a long time period and sampling the alignment periodically. There was a good fit indicating the reliability of the stationary probability distribution found using the F-P equation. Using the backwards Kolmogorov equation I derived formulae for the moments of the first passage time specifically looking at the mean first passage time, which indicates how often the alignment switches from positive to negative and vice versa. This is a useful indication of how locked-in to a particular direction the locusts are: the smaller the switching time the less stable that particular aggregation of locusts is. I gave two reliable (a long time simulation and the exact formula derived from the backwards Kolmogorov equation) ways to calculate the switching time which gave results which differed first in the fourth significant figure, indicating their accuracy. I also gave two approximations to the mean switching time which, although less accurate, were faster and less numerically intensive to compute. I then introduced the concept of equation-free analysis, an incredibly powerful technique, that can be used to find the drift, diffusion and consequently potential, stationary probability distribution and mean switching time of a process which is assumed to have an underlying stochastic differential equation dictating its behaviour. To test the equation-free technique I used it on the example SDE, for which the potential and stationary probability distribution were already known; using the SDE as a 'black box' as if the underlying stochastic process was unknown. The potential given by the equation-free technique was an almost exact replication of known potential for the SDE and since formula for the mean switching time depends only on the potential, the potential match was assumed to be a good enough validation of the equation-free techniques.

In Chapter 3 I introduced Czirók's one dimensional self-propelled particle model used to simulate the locust experiment introduced earlier. I demonstrated that with the right choices of parameter values, the mean velocity of the particles in the model gave switching behaviour similar to that of the locust experiment and of the example SDE. This indicated that there was likely an underlying SDE modelling the behaviour of the mean velocity and

hence that equation-free techniques could be used to find the underlying properties of the SDE. I found the underlying potential and compared the mean switching time and the stationary probability distribution to those found by running the code for a long time again with favourable results. I also analytically derived the potential and stationary probability distribution for a specific case of the model and compared these to the equation-free results for the same special case. The similarity between the analytically derived and equation-free potential was astonishing, indicating that indeed there is an underlying SDE dictating the behaviour of the mean velocity of the particles in the model and that the equation-free methods were a powerful way to find the properties of this SDE. To confirm these findings further I introduced the long-time equation-free approach to find the properties of an underlying SDE, which gave good comparisons to the short-time equation-free results. The long-time equation-free method was also applied to the experimental results to give the potential and stationary probability distribution and although there was only limited data the result showed a double welled potential that the one dimensional model predicts. I have shown that the whole range of equation-free results are very useful for models and even for experimental data, in finding important properties of marching bands of animals such as locusts. The similarity between the experimental results and the model results are also a vindication of the SPP models.

In Chapter 4 I went on to describe the basics of evolutionary game theory including Nash equilibria and evolutionarily stable states as well as the four basic types of two participant games. I showed, using the replicator equation, that the four different games led to the evolution of markedly different populations. In order to apply this theory, in Chapter 5, I introduced the 2-D analogy of the 1-D Czirók SPP model; the Vicsek model . Initially I demonstrated that a phase change in the alignment of a group of self-propelled particles without a leader is exhibited when the interaction radius is varied. Although a phase change has been exhibited by varying the density and the noise of the particles a phase change from varying the IR has not been shown in the literature before, although it was expected as varying the IR of particles has a similar effect to varying the density. More importantly, when I introduced a leader particle to the Vicsek model I again found that a phase change was exhibited by varying the interaction radius, which is a truly original and unexpected result. I went on to explain how I aimed to evolve the particles to mimic as closely as possible natural selection, whilst keeping within the bounds of what could reasonably be achieved. I drew up an invasion table in an attempt to find the ESS (choice of interaction radius) and concluded that the interaction radius which was the best estimate to the ESS was small, as opposed to the optimum interaction radius, which gave the largest average payoff, which was found to be large. (specifically I found $r = 1$ to be the closest approximation to the ESS (see Appendix B)) [1]. This conclusion enabled me to disprove David Sumpter's hypothesis that the interaction radius that would be favoured by natural selection would be in the region for which the phase change occurred: The interaction radius evolved to be small despite all the particles doing better when they all shared a large interaction radius. I went on to explain this counter-intuitive result using the description of movies which showed the interactions of particles with a mix of large and small interaction radii. I explained in game theoretic terms how these interactions gave rise to the evolution of a small interaction radius.

Overall the project has given an insight into the varied use of self-propelled particle

[1] This conclusion was of course prefaced by warnings that the ESS may not be a pure strategy at all or indeed any of the few different IR that I tried, but this was the best approximation to it.

models from evolutionary game theory through to modelling locusts in the field. It has introduced some powerful techniques that have been applied to the models to find properties that otherwise would be unattainable and given some counter intuitive results that would not have been predicted without them.

6.1 Further Work

Throughout the project there have been several areas where I have had to amend my work for one reason or another. One example of this is in applying the equation-free techniques to the experimental data. Ideally the experiments would be run for a longer time (in order to gain a more accurate potential for middling alignment values) and with a greater number of variations in the densities of locusts used. This would enable a more accurate application of the long-time equation-free technique (see Section 3.5). By far the area with the largest potential for expansion is the application of evolutionary game theory to the self-propelled particle models, where I have really only scratched the surface. There are possibilities of adding mutation to the model and changing the strength of the selection in order to see if low interaction radii are still favoured. There are also a whole range of biologically motivated initialisations for the range of interaction radii of the particles, which could give different types of evolution under different circumstances. The very fact that the range of interaction radii is continuous not discrete (let alone varying particle number, domain size and noise) means that there are no end of possibilities to the extensions that could be made to the project. However, in this project I have managed to reduce the possibilities by modelling and evolving particles in two dimensions and finding the region in which the optimum interaction radius lies. In using evolutionary game theory I have explained how counter-intuitive results, that might come about from evolving the particles, can be justified, giving possible extensions to the project a solid base from which to launch.

Chapter 7

Appendices

7.1 Appendix A-Derivation of the Backwards Kolmogorov Equation

The intuitive Chapman-Kolmogorov equation (2.5.2) can be re-written in the form,

$$P(y,t|x,s-\Delta s)=\int_{\mathbb{R}}P(y,t|z,s)P(z,s|x,s-\Delta s)dz, \tag{7.1.1}$$

where Δs is small and $s<t$. Taylor-expanding $P(y,t|z,s)$ about $z=x$ assuming that $|z-x|$ is also small. (This is a reasonable assumption since it is also assumed Δs is small: The process cannot have gone far in this small time and hence z is close to x.)

$$P(y,t|z,s)=P(y,t|x,s)+(z-x)\frac{\partial P}{\partial x}(y,t|x,s)+\frac{(z-x)^2}{2}\frac{\partial^2 P}{\partial x^2}(y,t|x,s)+O(|z-x|^3). \tag{7.1.2}$$

Substituting (7.1.2) into the C-K equation (7.1.1) gives:

$$\begin{aligned}P(y,t|x,s-\Delta s)&=\int_{\mathbb{R}}[P(y,t|x,s)+(z-x)\frac{\partial P}{\partial x}(y,t|x,s)\\&+\frac{(z-x)^2}{2}\frac{\partial^2 P}{\partial x^2}(y,t|x,s)+O(|z-x|^3)]P(z,s|x,s-\Delta s)dz\\&=P(y,t|x,s)+\int_{\mathbb{R}}(z-x)P(z,s|x,s-\Delta s)dz\,\frac{\partial P}{\partial x}(y,t|x,s)\\&\quad+\int_{\mathbb{R}}\frac{(z-x)^2}{2}P(z,s|x,s-\Delta s)dz\,\frac{\partial^2 P}{\partial x^2}(y,t|x,s).\end{aligned} \tag{7.1.3}$$

The right hand side of (7.1.3) comes from taking functions that are not dependent on z out of the integrals and simplifying. Recall the original SDE (2.3.2). Substitute this in to (7.1.3) and simplify in an entirely analogous manner to that of the derivation of the F-P equation (see Section 2.5) to give:

$$P(y,t|x,s-\Delta s)=P(y,t|x,s)+f(x)\Delta s\frac{\partial P}{\partial x}(y,t|x,s)+D(x)\Delta s\frac{\partial^2 P}{\partial x^2}(y,t|x,s)+O(\Delta s^2). \tag{7.1.4}$$

Dividing through by Δs and taking the limit as $\Delta s\to 0$ in (7.1.4) gives the backwards Kolmogorov equation:

$$\frac{\partial P}{\partial t}(y,t|x,s)=f(x)\frac{\partial P}{\partial x}(y,t|x,s)+D(x)\frac{\partial^2 P}{\partial x^2}(y,t|x,s) \tag{7.1.5}$$

7.2 Appendix B-Further Investigation into the Evolutionarily Stable Radius

The invasion matrix (Table 5.1 page 55) indicates that the evolutionarily stable IR will be found in the region around $r = 1$. Since IR $r = 0$ was only invaded twice in total I will choose the region between $r = 0$ and $r = 1.25$ to investigate further. I will create another invasion table over this smaller range if interaction radii.

		1 particle					
	Interaction radius	0	0.25	0.5	0.75	1	1.25
79 particles	0	-	$\frac{1}{80}$	$\frac{6}{80}$	$\frac{0}{80}$	$\frac{0}{80}$	$\frac{1}{80}$
	0.25	$\frac{2}{80}$	-	$\frac{1}{80}$	$\frac{1}{80}$	$\frac{1}{80}$	$\frac{1}{80}$
	0.5	$\frac{1}{80}$	$\frac{2}{80}$	-	$\frac{1}{80}$	$\frac{1}{80}$	$\frac{0}{80}$
	0.75	$\frac{0}{80}$	$\frac{0}{80}$	$\frac{0}{80}$	-	$\frac{2}{80}$	$\frac{2}{80}$
	1	$\frac{0}{80}$	$\frac{0}{80}$	$\frac{0}{80}$	$\frac{0}{80}$	-	$\frac{0}{80}$
	1.25	$\frac{0}{80}$	$\frac{0}{80}$	$\frac{0}{80}$	$\frac{0}{80}$	$\frac{1}{80}$	-

Table 7.1: *A table to demonstrate strategy invasion between smaller IR. The vertical column is the IR of the particles which started with 79 particles and the horizontal row indicates the IR of particles which started with just one particle.*

It is clear to see from Table 7.1 above that the best estimate of the evolutionarily stable interaction radius is $r = 1$. However, it should be noted that since I have only used a finite range of interaction radii, I can not be sure that $r = 1$ is the exact ESS. It should also be noted that the ESS may not be a pure strategy at all. It may turn out to be a mixed strategy, so that an evolutionarily stable population has a mix of particles with various different interaction radii. However, given the computationally intensive nature of the simulations and the infinity of possible mixed strategies, $r = 1$ is the closest estimate available to the ESS.

Bibliography

[1] M. Aldana, V. Dossetti, C. Huepe, V. M. Kenkre, and Larralde H. Phase Transitions in Systems of Self-Propelled Agents and Related Network Models. *Physical Review Letters, The American Physical Society*, 98(9), March 2007.

[2] R Ardrey. *The Social Contract: A Personal Inquiry into the Evolutionary Sources of Order and Disorder*. Doubleday, 1st edition, June 1971.

[3] S. Bazazi, J. Buhl, J.J. Hale, M.L. Anstey, G.A. Sword, S.J. Simpson, and I.D. Couzin. Collective motion and cannibalism in locust marching bands. *Submitted*, 2007.

[4] J. Buhl, D.J.T. Sumpter, I.D. Couzin, J.J. Hale, E. Despland, E.R. Miller, and S.J. Simpson. From Disorder to Order in Marching Locusts. *Science*, 312:1402–1406, June 2006. www.sciencemag.org.

[5] T.M. Caro. The functions of stotting in Thomson's gazelles: some tests of the predictions. *Animal Behaviour*, 34(33):663–684, 1986.

[6] I Couzin, J Krause, N.R. Franks, and S.A. Levin. Effective leadership and decision making in animal groups on the move. *Nature*, 433:513–516, February 2005.

[7] A. Czirók, A.-L. Barabási, and T. Vicsek. Collective Motion of Self-Propelled Particles: Kinetic Phase Transition in One Dimension. *Physical Review Letters, The American Physical Society*, 82(1):209–212, January 1999.

[8] R. Dawkins. *The Selfish Gene*. OUP, 2nd edition, 1999.

[9] R. Erban, I.D. Couzin, C. Escudero, T.A. Frewen, I.G. Kevrekidis, P.K. Maini, and D.J. Sumpter. In preparation. October 2006.

[10] R. Erban, I. Kevrekidis, D. Adalsteinsson, and T. Elston. Gene Regulatory Networks: A Coarse-Grained Equation Free Approach to Multiscale Computation. *The Journal Of Chemical Physics*, 124(084106), 2006.

[11] C.D. FitzGibbon and J.H. Fanshawe. Stotting in Thomson's gazelles: an honest signal of condition. *Behavioural Ecology and Sociobiology*, 23(2):69–74, May 1988.

[12] Food and Agriculture Organisation of the United Nations. *Desert Locust Guidelines*. Five volumes, 1994. Rome.

[13] R.F. Fox. Functional-calculus approach to stochastic differential equations. *Physical Review A*, 33(1):467–476, January 1986.

[14] D.T. Gillespie. *Markov Processes, An Introduction for Physical Scientists*. Academic Press, Inc., Harcourt Brace Jovanovich, Academic Press Limited, 24-28 Oval Road, London, NW1-7DX, 1992.

[15] G. Grégoire and H. Chaté. Onset of Collective and Cohesive Motion. *Physical Review Letters, The American Physical Society*, 96(2), January 2004.

[16] M. Haataja, D.J. Srolovitz, and I.G. Kevrekidis. Apparent Hysteresis in a Driven System with Self-Organized Drag. *Physical Review Letters, The American Physical Society*, 92(16), April 2004.

[17] D.J. Higham. An Algorithmic Introduction to Numerical Simulation of Stochastic Differential Equations. *SIAM Review*, 43(3):525–546, 2001.

[18] D.J. Higham and N.J. Higham. *Matlab Guide*. SIAM, 2nd edition, 2005.

[19] J. Hofbauer and K. Sigmund. *Evolutionary Games and Population Dynamics*. CUP, 1st edition, 1998.

[20] S. Howison. *Practical Applied Mathematics*. Cambridge Texts in Applied Mathematics. CUP, The Edinburgh Building, Cambridge, CB2 2RU, UK, 1st edition, 2005.

[21] S. Mu, T. Chu, and L. Wanga. Coordinated Collective Motion in a Motile Particle Group With a Leader. *Physica A: Statistical Mechanics and its Applications*, Volume 351(2-4):211–216, June 2005.

[22] S.J. Simpson, G.A. Sword, P.D. Lorch, and I.D. Couzin. Cannibal crickets on a forced march for protein and salt. *PNAS*, 103(11):4152Ű4156, March 2006.

[23] N. Smythe. On the Existence of "Pursuit Invitation" Signals in Mammals. *American Naturalist*, pages 491–494, 1970.

[24] B. Stonehouse and C.M. Perrins. *Reliability in Communication Systems and the Evolution of Altruism in Evolutionary Ecology*. Macmillan, 1977. 253-259.

[25] N.G. van Kampen. Itô Versus Stratonovich. *Journal of Statistical Physics*, 24(1):175–187, 1981.

[26] T. Vicsek, A. Czirók, E. Ben-Jacob, I. Cohen, and O. Shochet. Novel Type of Phase Transition in a System of Self-Driven Particles. *Physical Review Letters, The American Physical Society*, 75(6):1226–1229, August 1995.

[27] A.J. Wood and G.J. Ackland. Evolving the selfish herd: emergence of distinct aggregating strategies in an individual-based model. *Proceedings of the Royal Society B*, March 2007. Published online.